THE ASTROPHYSICAL JOURNAL, 310:291–316, 1986 November 1

X-RAY SPECTRA OF PG QUASARS. I. THE CONTINUUM FROM X-RAYS TO INFRARED[1]

MARTIN ELVIS
Harvard-Smithsonian Center for Astrophysics
RICHARD F. GREEN
Kitt Peak National Observatory, National Optical Astronomy Observatories[2]
JILL BECHTOLD
Steward Observatory, University of Arizona
MAARTEN SCHMIDT, G. NEUGEBAUER, B. T. SOIFER, AND K. MATTHEWS
Palomar Observatory, California Institute of Technology
AND
G. FABBIANO
Harvard-Smithsonian Center for Astrophysics
Received 1985 November 7; accepted 1986 April 16

ABSTRACT

We present *Einstein* IPC X-ray spectra for a sample of eight optically selected quasars from the Palomar Bright Quasar Survey. The quasars have a mean power-law energy slope (0.2–4.0 keV) of $\alpha_E = 1.05$ with an observed dispersion of 0.25, and none shows evidence for low-energy absorption above the Galactic value. In five individual cases α_E is inconsistent at 90% confidence with the 0.7 value found in active galactic nuclei selected for being bright in hard X-rays. This difference in slope is shown to be most likely due to the hard X-ray selection criterion rather than luminosity, redshift, or $U-B$ color. Energy range differences may also contribute. New *IUE* and optical continuum spectra and infrared photometry are presented for these quasars. The data are combined into log νf_ν versus log ν distributions from the X-ray regime into the infrared. These continuum plots support the decomposition of the overall quasar spectrum into a power law plus a superposed optical-UV "big bump," which may be due to an accretion disk. At least six of the quasars have $\nu f_\nu \approx$ constant between their infrared and X-ray power laws, suggesting a strong link between the two regions and possibly that a single mechanism produces a power law across five decades of frequency. Possible emission mechanisms are discussed.

Subject headings: quasars — radiation mechanisms — spectrophotometry — ultraviolet: spectra — X-rays: spectra

I. INTRODUCTION

To understand the nature of the highly luminous continuum is a primary goal of quasar research. The ability of the *Einstein* imaging proportional counter (IPC) to determine the soft X-ray spectra of faint X-ray sources enables a new perspective to be taken of the overall continuum shape of quasars.

Earlier X-ray spectra of emission-line active galaxies in the 2–20 keV band (Mushotzky *et al.* 1980; Mushotzky and Marshall 1980; and Mushotzky 1982) could almost all be described by a single power law with differing amounts of low-energy absorption. The energy spectral index α_E ($F_\nu \propto \nu^{-\alpha_E}$) of this power law is highly uniform, with a mean value of ~ 0.7. The observed dispersion in α_E is probably less than 0.1 (Mushotzky 1984). This result holds for 30 active galactic nuclei (AGNs), which span a luminosity range of 10^3, and for both radio-loud and radio-quiet objects. The spectra are also consistent with the same slope continuing out to 120 keV for the 11 active galaxies detected at higher energies (by *HEAO 1* A-4, Rothschild *et al.* 1983). *Einstein* solid state spectrometer (SSS) observations (Petre *et al.* 1984) appear to show that the same slope continues for 15 of these AGNs into the softer (0.75–4.5 keV) X-ray region. Some exceptions have been reported, the most significant being some low-energy observations that show a "soft excess" over the canonical power law below ~ 1 keV. Such excesses are relatively infrequent. Preliminary *EXOSAT* results (Pounds 1985) indicate that $\alpha_E \approx 0.7$ continues to ~ 0.15 keV for 14 of 15 AGNs taken from 2–20 keV surveys. Only one object showed a soft excess.

The widespread uniformity of these spectra has naturally led to the suggestion that a "canonical X-ray spectrum" may exist for active galaxies and quasars. This in turn has led to many theoretical efforts to produce naturally a narrow range of slopes centered on 0.7 (Mészáros 1983; Kazanas 1984; Schlosman, Shaham, and Shaviv 1984; Zdziarski and Lightman 1985). However, the AGNs for which X-ray spectra exist are almost all hard X-ray selected and so are the brightest objects in the hard X-ray (2–20 keV) sky. This may make them a biased sample of the general AGN population.

For quasars selected by optical or radio techniques, the first IPC spectra have shown that the "canonical spectrum" picture is not a general property of all AGNs (Elvis, Wilkes, and Tananbaum 1985), at least in the low-energy range. The three quasar spectra published by Elvis *et al.* have best-fit power-law spectral indices of $\alpha_E \approx 0.6$, ~ 1.2, and ~ 2.2. In one case (PG 1211+143), no single power law gives an acceptable

[1] Based on data acquired with the *Einstein Observatory*, the Hale 5 m telescope at Palomar Observatory, and the *International Ultraviolet Explorer* satellite, which is operated at the Goddard Space Flight Center for the National Aeronautics and Space Administration.

[2] NOAO is operated by the Association of Universities for Research in Astronomy, Inc., under contract with the National Science Foundation.

fit when the 6 keV MPC observation is included. From such a small sample it is impossible to tell whether there are distinct groups of indices or whether a continuous distribution of slopes exists.

In this paper we present IPC X-ray spectra for an additional eight quasars. These are all members of the Palomar Bright Quasar Survey (Schmidt and Green 1983), which is subset of the Palomar-Green catalog of ultraviolet-excess stellar objects (Green, Schmidt, and Liebert 1986, hereafter PG). The PG quasars were selected optically to have $B \lesssim 16.16$ and $U-B < -0.44$, in a region of sky with $|b| > 30°$. These eight quasars were the first PG quasars with adequate counting statistics for which the IPC data were calibrated for spectral work. We find that these quasars have, on average, steeper X-ray spectra than the "canonical" 0.7 value. We have therefore included observations of these objects at ultraviolet, optical, and infrared (UVOIR) frequencies to allow a broad-band study of their continua.

In a separate paper (Green *et al.* 1985, hereafter Paper III) we will examine the line and continuum cooling radiation of these and other PG quasars and their relation to continuum properties. One other PG quasar (PG 1211+143; Elvis, Wilkes, and Tananbaum 1985) has such an unusually steep X-ray spectrum (and the highest L_x/L_{opt} in the bright quasar sample) that it will be discussed separately (Bechtold *et al.* 1985, hereafter Paper II).

A Hubble constant of 50 km s^{-1} Mpc^{-1} is used throughout.

II. OBSERVATIONS

a) Einstein X-Ray Spectra

At X-ray luminosities greater than $\sim 10^{44}$ ergs s^{-1} (2–10 keV),[3] low-energy photoelectric absorption is rarely seen (Lawrence and Elvis 1982; Petre *et al.* 1984). This allows the study of the X-ray continua of quasars with detectors sensitive to low energies, like the *Einstein* imaging proportional counter (IPC, Gorenstein, Harnden, and Fabricant 1981).

The X-ray observations reported here were made with the *Einstein Observatory* (*HEAO 2*; Giacconi *et al.* 1979). The X-ray detections of these and many other PG quasars are reported in Tananbaum *et al.* (1986). Table 1 gives the observing log for the eight quasars in our study for each wavelength band observed, together with the redshift and absolute magnitudes of the quasars from Schmidt and Green (1983). Schmidt and Green have adopted the criterion $M_B < -23$ for terming an AGN a quasar. This criterion is to some extent arbitrary, but it is observationally convenient since for such absolute magnitudes any underlying galaxy contribution is small. The same criterion is used in the catalog of Véron-Cetty and Véron (1985). Five of our eight objects satisfy this criterion (Table 1). Further details of the *Einstein* observations are given in Table 2. Since the quality of an IPC fit is limited by the total net source counts and that of the MPC by the count rate of the source, Table 2 lists these quantities.

i) *IPC Spectra*

The primary instrument used was the IPC, which has a broad bandpass ($\sim$0.1–4.0 keV), limited intrinsic energy resolution ($E/\Delta E \approx 1$), and a 1′ beam size (Gorenstein, Harnden, and Fabricant 1981). The recent calibration of the IPC (Harnden and Fabricant 1986) has allowed the use of this resolution for deriving the spectra of bright on-axis point sources. Spectral slopes can be derived for quasars with $\gtrsim 500$ counts. The pulse height analysis (PHA) channels spanning the range 0.1–4.0 keV were used. This is typically 10 of the 16 available PHA channels. Source counts were taken from a circle of 3′ (22.5 pixels) radius centered on the source position. Background counts were taken from an annulus with the same center and with inner and outer radii of 5′ (37.5 pixels) and 6′ (45 pixels) respectively. The total number of background counts in the 0.1–4.0 keV band is small relative to the source counts. Within the 3′ radius source circle, a typical background rate is $\sim$40 counts (1000 s)$^{-1}$. This amounts to only 5%–15% of the source counts (Table 2).

PG 1545+210 was observed twice (Table 1). Table 2 gives details of the separate observations. Since the two spectral fitting contours overlap and there is no evidence for count rate variability, a spectrum was also fitted to the sum of the two observations. We use this summed spectrum in the following discussion.

We note that PG quasars in general do not lie in rich clusters of galaxies (Yee and Green 1984). It is unlikely that the small groups in which they are found would themselves be significant X-ray sources. The most luminous of these groups have luminosities $\sim$1/10 those of the quasars (Kriss, Cioffi, and Canizares 1983); typical groups are 100 times less luminous than the quasars.

ii) *Joint IPC/MPC Spectra*

The 2–7 keV count rate measured in the *Einstein* monitor proportional counter (MPC) was also used for the brighter sources. The MPC was a nonimaging instrument co-aligned with the *Einstein* mirror and provided high-energy data with reduced sensitivity (Halpern 1982). The MPC field of view was roughly coextensive with that of the IPC. At the flux levels of even the brightest quasars considered here, $\sim$1/2–1 UFU,[4] the MPC background subtraction procedure is sufficiently uncertain that MPC spectra cannot yet be reliably derived. Halpern (1982) has published MPC spectra for the four quasars we report on here. However, he used an earlier version of the background prediction data base. We have repeated his analysis with the final data base using the lowest six MPC pulse height channels. The best-fit spectral slopes from this procedure range over ± 0.5 of his value. This dispersion is sufficiently large that spectra from the MPC are unreliable at these flux levels. We do not feel confident that our new fits are substantially more reliable than those of Halpern. For some of the quasars, however, the MPC unambiguously detects the object and thus can be used to determine a flux point in the hard X-ray band. This is valuable in limiting the allowed range of power-law indices. We used only the total count rate from channels 3–5 ($\sim$2.4–7.1 keV; Halpern 1982, Fig. 2.1), where the MPC is most sensitive.

The determination of source fluxes in the MPC relies on the ability to predict the background count rates in each of the PHA channels. When tested against the observed background during long pointings at effectively empty Deep Survey fields, the background predictions are found to have a scatter of $\sim$1%–2% in each channel. The total background rate in chan-

[3] L_x(2–10 keV) = L_x(0.3–3.5 keV) for $\alpha_E = 0.7$
= 1.5L_x(0.3–3.5 keV) for $\alpha_E = 1.0$,
both with no low-energy cutoff.

[4] 1 UFU = 1 *Uhuru* flux unit = 2.4×10^{-11} ergs cm^{-2} s^{-1} (2–10 keV) (Forman *et al.* 1978) $\approx$ 1 μJy, at 2 keV.

TABLE 1

LOG OF OBSERVATIONS

PG	NAME	z[a]	m_B[a]	M_B[a]	log $(4\pi D^2)$[b]	DATES OF OBSERVATIONS				
						IUE LWR	*IUE* SWP	Optical	IR	*Einstein*
0049+171.....	Mrk 1148	0.064	15.9	−22.07	55.271	...	...	1980 Nov 13	1980 Jul 2	1980 Jun 21
1202+281.....	GQ Comae	0.165	15.0	−25.03	56.135	1983 Jan 20	1980 May 3	1980 Nov 14	1980 May 31	1979 May 23
1244+026.....	...	0.048	16.2	−21.17	55.014	1983 Feb 8	1983 Feb 8	1980 Jul 18	1980 Jul 2	1980 Jul 12
1307+085.....	...	0.155	15.3	−24.63	56.077	1984 Feb 21	1980 May 4	1980 Jul 19	1980 May 31	1981 Jan 27
1416−129.....	...	0.129	15.5	−24.10	55.907	1983 Jun 7	1980 Jul 4	1980 Jul 19	1980 May 31	1981 Jan 30
1426+015.....	Mrk 1383	0.086	15.1	−23.55	55.537	1983 Feb 6	1983 Feb 6	1980 Jul 18	1980 May 31	1980 Aug 3
1501+106.....	Mrk 841	0.036	15.1	−21.60	54.760	1983 Feb 6	1983 Feb 6[c]	1980 Jul 19	1980 May 28	1980 Jan 18
1545+210.....	3C 323.1	0.266	16.1	−25.08	56.590	1983 Jun 7	1983 Jun 6	1980 Jul 18	1980 May 31	1979 Aug 13 (seq 2054) 1979 Aug 30 (seq 2055)

[a] Schmidt and Green 1983. M_B is for $q_0 = 0.1$.

[b] $\log (4\pi D^2) = \log \left(z + \frac{1}{2} z^2 \right)^2 + \log 4\pi \left(\frac{cz}{H_0} \right)^2$ cm^2, for $H_0 = 50$ km s^{-1} Mpc^{-1}, $q_0 = 0$, $\Lambda = 0$.

[c] Two observations.

TABLE 2

Einstein IPC AND MPC X-RAY OBSERVATIONS

PG	Name	N_H (gal)[a] ($\times 10^{20}$)	Observation Sequence Number	IPC Observing Time (s)	Effective IPC Instrumental Gain	Net IPC Counts	IPC Counts s^{-1}	MPC Counts s^{-1}	MPC Observing Time (s)
0049+171	Mrk 1148	4.3	8431	1373	15.0	510 ± 23	0.37 ± 0.02	0.49 ± 0.08	1436
1202+281	GQ Comae	1.7	4258	4176	11.8	1080 ± 35	0.26 ± 0.01	...	...
1244+026	...	1.8	8433	1232	15.4	400 ± 21	0.32 ± 0.02	...	...
1307+085	...	2.1	5344	2149	17.6	598 ± 26	0.28 ± 0.01	...	...
1416−129	...	6.8	10373	2375	17.8	678 ± 28	0.29 ± 0.01	0.62 ± 0.08	2537
1426+015	Mrk 1383	2.8	5348	2034	14.0	1350 ± 38	0.66 ± 0.02	0.41 ± 0.07	1810
1501+106	Mrk 841	2.4	6713	1475	17.0	1699 ± 42	1.15 ± 0.03	0.76 ± 0.08	1677
1545+210	3C 323.1	4.3							
A.....	...	...	2054	1912	16.4	430 ± 23	0.22 ± 0.01	...	...
B.....	...	...	2055	1541	12.6	323 ± 19	0.21 ± 0.01	...	...
Sum	...	...	...	3453	14.8	753 ± 30	0.22 ± 0.01	...	...

[a] Interpolated from Stark *et al.* 1985.

nels 3–5 is $\sim$4.5 counts s^{-1}, so that the predicted background, and hence the net counts in the source, are uncertain by $\sim$0.07 counts s^{-1}. These errors dominate the uncertainties in determining the MPC flux of weak sources such as the quasars discussed here (see Table 2). These background prediction uncertainties have been included in quadrature in the error on the MPC source counts (as given in Table 2). In addition, the relative calibration of the MPC and IPC is determined to $\lesssim$10% (Appendix A), and so we have included a 10% error on the MPC count rate to allow for this. In order to fit spectra to the combined IPC/MPC data, we folded identical spectra through each instrument. We then added the resulting χ^2 to that obtained from the IPC fit.

The MPC count rates are unlikely to be contaminated by other X-ray sources. No other source is seen in any of the IPC fields above 1/10 of the quasar count rate. Extra IPC sources are only seen in two fields, those of PG 1202+281 (one 72 count source) and PG 1545+210 (one 14 count source in the "2054" observation).

iii) *Fitted Spectral Forms*

For each quasar we attempted to fit simple models of the form (1) power law, (2) thermal bremsstrahlung (exponential plus Gaunt factor), (3) thermal plasma (Raymond and Smith 1977; Raymond 1980), (4) black body. The column density N_H of cold absorbing material at cosmic abundance (using cross sections from Brown and Gould 1970) in front of the source was also allowed to vary simultaneously. Fits to each model were made for the IPC alone and, where possible, to the combined IPC/MPC data.

Table 3 gives the minimum χ^2 (not reduced) for each form of fit for each quasar and the number of degrees of freedom in each fit. In parentheses we give the χ^2 for the fit when N_H is forced to exceed the minimum allowed Galactic column density. Both single power-law and thermal bremsstrahlung models give acceptable fits for all the quasars. In most cases both a Raymond thermal plasma and a blackbody spectrum fail to fit adequately, particularly if N_H is constrained to exceed the minimum Galactic column density (see below). For simplicity and ease of comparison with previous results, we discuss the results in terms of the power-law fits.

Table 4 gives the best-fit values for α_E and N_H in a single power-law fit. Values and ranges are given both for the IPC alone and for the IPC/MPC combination. Figure 1 shows the 90% confidence contour in (α_E, log N_H)-space for each quasar. The eight panels have different axis scales because of the varying quality of the fits. Again both the IPC alone and the joint IPC/MPC results are given. The vertical lines show

TABLE 3

CHI-SQUARE MINIMA FOR FITS TO X-RAY SPECTRA

PG	Name		Degrees of Freedom[a]	Power Law[b]	Exponential + Gaunt[b]	Raymond Thermal[b]	Blackbody[b]
0049+171.....	Mrk 1148	IPC	8	12.7 (12.7)	12.0 (12.0)	24.0 (28.6)	11.8 (14.4)
		IPC/MPC	9	12.9 (12.9)			
1202+281.....	GQ Comae	IPC	7	5.2 (5.2)	5.1 (5.4)	7.0 (31.7)	46.1 (50.8)
1244+026.....	...	IPC	9	7.6 (7.9)	8.7 (10.8)	23.5 (24.4)	18.9 (20.7)
1307+085.....	...	IPC	9	6.7 (8.0)	7.4 (14.7)	41.9 (85.1)	38.8 (45.2)
1416−129.....	...	IPC	9	7.9 (7.9)	6.0 (6.0)	6.3 (6.3)	5.6 (6.4)
	...	IPC/MPC	10	13.8 (13.8)			
1426+015.....	Mrk 1383	IPC	8	8.6 (8.6)	7.4 (7.4)	6.9 (19.2)	43.1 (66.3)
		IPC/MPC	9	9.2 (9.2)			
1501+106.....	Mrk 841	IPC	9	3.0 (3.0)	3.1 (7.8)	36.6 (127.0)	91.5 (126.7)
		IPC/MPC	10	3.1 (3.1)			
1545+210.....	3C 323.1	2054 IPC	10	12.8 (14.2)	11.2 (16.7)	10.0 (32.0)	18.8 (20.7)
		2055 IPC	8	5.9 (5.9)	4.5 (4.5)	3.9 (9.5)	5.7 (6.4)
		Sum IPC	8	7.4 (7.4)	5.5 (10.8)	5.5 (31.5)	13.9 (26.1)

[a] Degrees of freedom in fit = number of PHA channels − 2 fit parameters.

[b] Values in parentheses are for $N_H > [N_H \text{ (gal)} - 10^{20}]$.

TABLE 4

SINGLE POWER-LAW FITS TO PG QUASAR X-RAY SPECTRA

		IPC FITS				JOINT IPC/MPC FITS			
PG	NAME	α_E	N_H ($\times 10^{20}$)	$\alpha_E[N_H > N_H(\text{gal})]$	Intrinsic N_H ($\times 10^{20}$)	α_E	N_H ($\times 10^{20}$)	$\alpha_E[N_H > N_H(\text{gal})]$	Intrinsic N_H ($\times 10^{20}$)
0049+171...	Mrk 1148	$0.7^{+3.0}_{-0.4}$	6.0^{+50}_{-4}	$0.70^{+3.0}_{-0.4}$	<53	$0.95^{+0.6}_{-0.4}$	9^{+5}_{-7}	$0.95^{+0.6}_{-0.4}$	<10
1202+281...	GQ Comae	$1.1^{+0.3}_{-0.5}$	$3.0^{+1.0}_{-3.0}$	$1.1^{+0.3}_{-0.4}$	<5	...	...	...	...
1244+026...	...	$1.5^{+1.3}_{-0.5}$	$1.0^{+5.0}_{-1.0}$	$1.5^{+1.3}_{-0.3}$	<5	...	...	...	...
1307+085...	...	$1.0^{+0.6}_{-0.3}$	$0.6^{+3.4}_{-0.6}$	$1.2^{+0.4}_{-0.1}$	<1	...	...	...	...
1416−129...	...	$1.9^{+1.4}_{-1.2}$	40.0^{+50}_{-32}	$1.9^{+1.4}_{-1.2}$	<90	$0.95^{+0.8}_{-0.5}$	15^{+25}_{-10}	$0.95^{+0.8}_{-0.5}$	<35
1426+015...	Mrk 1383	$1.3^{+0.4}_{-0.4}$	$3.5^{+1.5}_{-2.0}$	$1.3^{+0.4}_{-0.3}$	<3	$1.3^{+0.3}_{-0.3}$	$3.5^{+1.5}_{-2.0}$	$1.3^{+0.3}_{-0.3}$	<2
1501+106...	Mrk 841	$1.0^{+0.3}_{-0.3}$	$1.3^{+1.2}_{-1.3}$	$1.0^{+0.3}_{-0.05}$	<1	$1.0^{+0.2}_{-0.2}$	$1.3^{+0.7}_{-1.3}$	$1.0^{+0.20}_{-0.05}$	<0.6
1545+210...	3C 323.1								
2054.....	...	$0.75^{+0.7}_{-0.5}$	$2.0^{+6.0}_{-2.0}$	$0.75^{+0.7}_{-0.4}$	<5	...	...	...	...
2055.....	...	$1.0^{+1.3}_{-0.5}$	$5.6^{+26}_{-4.7}$	$1.0^{+1.3}_{-0.5}$	<29	...	...	...	...
Sum.....	...	$0.75^{+0.55}_{-0.55}$	$3.0^{+4.0}_{-3.0}$	$0.75^{+0.55}_{-0.3}$	<4	...	...	...	...

NOTE.—90% two-parameter errors, $\chi_{\min}^2 + 4.6$ (Avni 1976).

the nominal galactic N_H interpolated from the Bell Labs survey (Stark *et al.* 1986) for each quasar with their 90% errors ($\pm 1 \times 10^{20}$ atoms cm^{-2}, Appendix B). Table 4 includes the value and allowed range of α_E, subject to the constraint that $N_H \geq [N_H(\text{Galactic}) - 10^{20}]$, i.e., that the minimum absorbing column density due to the Galaxy is met or exceeded. The maximum allowed value of N_H in excess of the minimum Galactic value is also listed in Table 4 as "Intrinsic N_H." In no case is an intrinsic column required in these quasars, so these values are all upper limits.

Since in at least one quasar (PG 1211+143; Elvis, Wilkes, and Tananbaum 1985; Paper II) the MPC flux lies above any extrapolation of a single power law, there is concern that the inclusion of MPC data in a single power-law fit is misleading. Arnaud *et al.* (1985) have also suggested that a two-component fit is needed to explain their *EXOSAT* spectrum of PG 1501+106. However, in none of the four cases in which a joint IPC/MPC fit has been made does a significantly poorer χ^2 result (Table 3). In three of the four cases (PG 0049+171, 1426+015, 1501+106) the best-fit value of α_E is not changed by more than 0.25. For these quasars the only effect of the MPC data point is to reduce the size of the allowed region of χ^2 space (shaded areas of Figs. 1*a*, 1*f*, and 1*g*), suggesting that the same power law seen in the IPC extends to at least 6 keV.

The soft excess seen by Arnaud *et al.* is not well constrained in form but is unlikely to make a significant contribution above 0.4 keV (see their Fig. 6). In their two-power-law fit, the soft component contributes no more than ~10% of its 0.2 keV count rate at 0.4 keV. This softness allows us to make a further test for a steep low-energy component by restricting the IPC data used in the joint fit to energies above ~0.6 keV. Although the IPC energy resolution is poor, the strong dip in its effective area immediately above 0.28 keV (due to the carbon edge) makes any contribution from photons below 0.6 keV very small in this fit. When we do this we find once again that the best-fit values remain unchanged in three of four cases and the allowed region of χ^2 space changes little except to leave the lower bound of N_H indeterminate (dashed contour in Figs. 1*a*, 1*f*, and 1*g*). Values of α_E steeper than 0.7 are still required for PG 1426+015 and PG 1501+106 at better than 90% confidence. For PG 1501+106 this high-energy IPC plus MPC fit is marginally inconsistent with the Arnaud *et al.* fit. The two 90% contours do not quite touch at the minimum N_H value, so the probability of their being consistent is, roughly, $\lesssim 1\%$ (in Fig. 1*g* the *EXOSAT* 90% steepest bound on α_E would form an essentially horizontal line at $\alpha_E = 0.8$). This is weak evidence for spectral variability in PG 1501+106. The normalization of our fit is very similar to that of Arnaud *et al.*, our value being ~25% higher at 2 keV.

The χ^2 plots for one quasar, PG 1416−129, are suggestive of a soft excess below 0.6 keV and a flatter continuum dominating at higher energies. Figure 1*e* shows the joint fit over the whole energy range to be similar to that of PG 0049+171 (Fig. 1*a*). When only the high-energy data are included, the best fit shifts to flatter slopes. The high-energy fit excludes slopes steeper than 0.85 at 90% confidence. Unfortunately, the combination of counting statistics and energy resolution does not allow us to decide between two components or a single power law over the whole energy range.

Although we cannot rule out more complex, two-component, forms for the quasar spectra, we discuss the data mainly in terms of the simplest, one-power-law parameterization. We use the joint IPC/MPC single power-law fit values for the full energy range with the requirement that N_H exceed the minimum Galactic N_H. Figure 2 shows this best fit compared with the raw count data for each quasar.

From the single power-law fits we can derive a number of useful fluxes and luminosities. These are given in Table 5. The errors on the fluxes are often highly asymmetric, since the best-fit values for the fluxes are often either the highest or lowest allowed values. The errors due to the uncertainty in the spectral fit have been added in quadrature to the uncertainties from the counting statistics of the detection. It is common for the steepest allowed spectrum to have the largest allowed flux. Table 5 gives the 0.3–3.5 keV broad-band flux and luminosity to allow direct comparison with other work, in particular the *Einstein* Medium Sensitivity Survey (Gioia *et al.* 1984). The flux density at 2 keV is useful for comparison with the large body of *Einstein* quasar work (e.g., Tananbaum *et al.* 1986; Marshall *et al.* 1984). In Table 5 we list in addition the spectrum normalization at 1 keV and the flux density at 0.2 keV. One keV lies near the peak of the IPC sensitivity and is the approximate "pivot point" for the spectral fits (see § III*b*[i] and Fig. 7). It is thus both relatively well determined and convenient for replotting the X-ray power-law fits. It is hoped that the 0.2 keV flux densities will be of use in making photoionization models of these quasars. For this purpose the lowest energy accessible is the most useful as it reaches closer to the

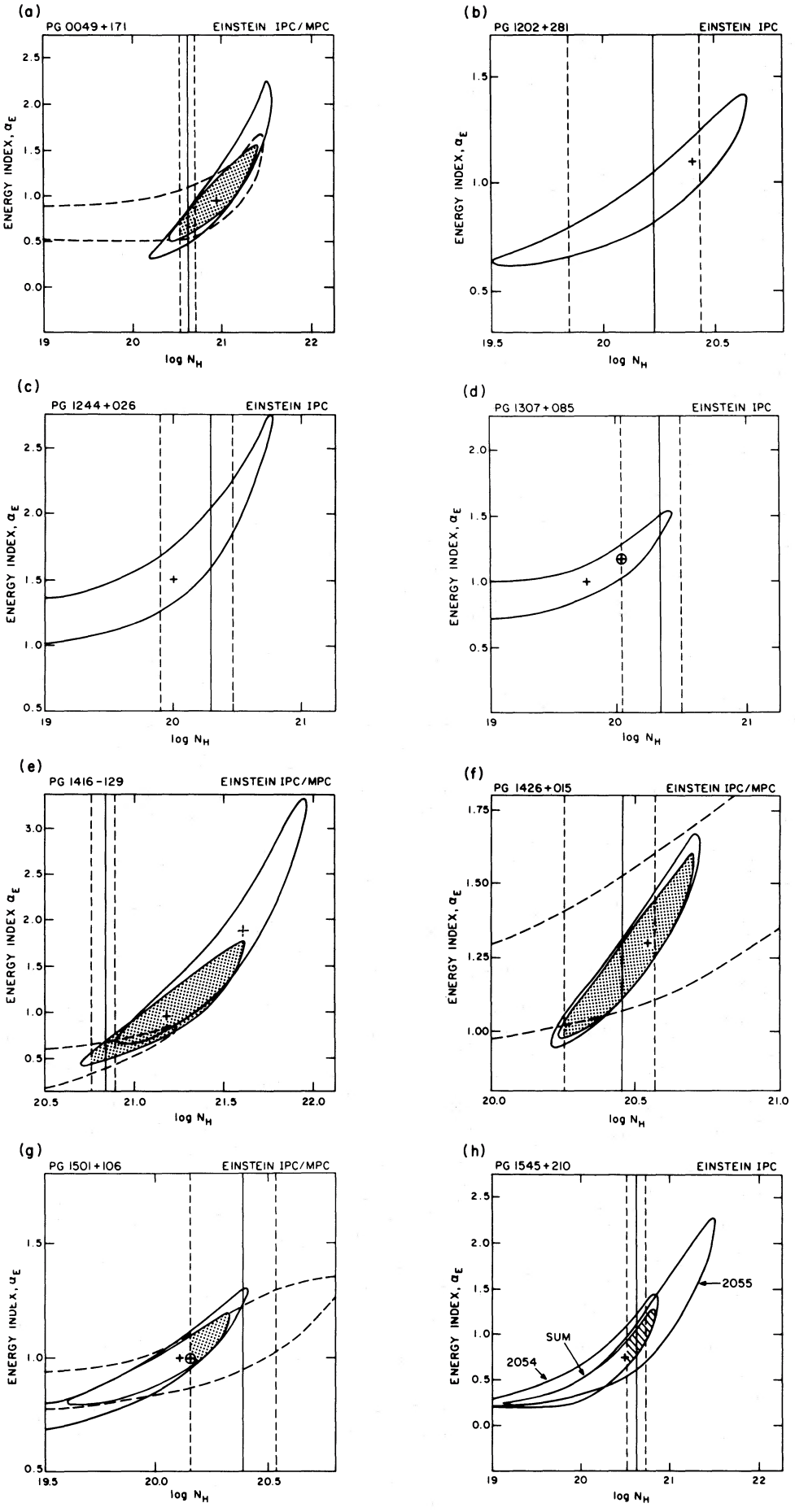

FIG. 1.—Allowed ranges of power-law index and N_H for the eight PG quasars. Chi-square contours at 90% confidence are shown in energy spectral index α_E vs. log column density N_H (atoms cm^{-2}) for power-law fits to the IPC (*open contours*) and to the joint IPC/MPC (*dotted areas*) data. The dashed contours are fits to the joint IPC/MPC data using only points above $\sim$0.6 keV. The vertical solid lines are the interpolated Stark *et al.* (1985) values of the column density due to our Galaxy. The vertical dashed lines are the Stark *et al.* values $\pm 10^{20}$ atoms cm^{-2}, which are 90% errors on this value (see Appendix B). For PG 1545+210, two separate IPC observations are shown as well as a joint fit to the sum of the two IPC observations (*hatched region*).

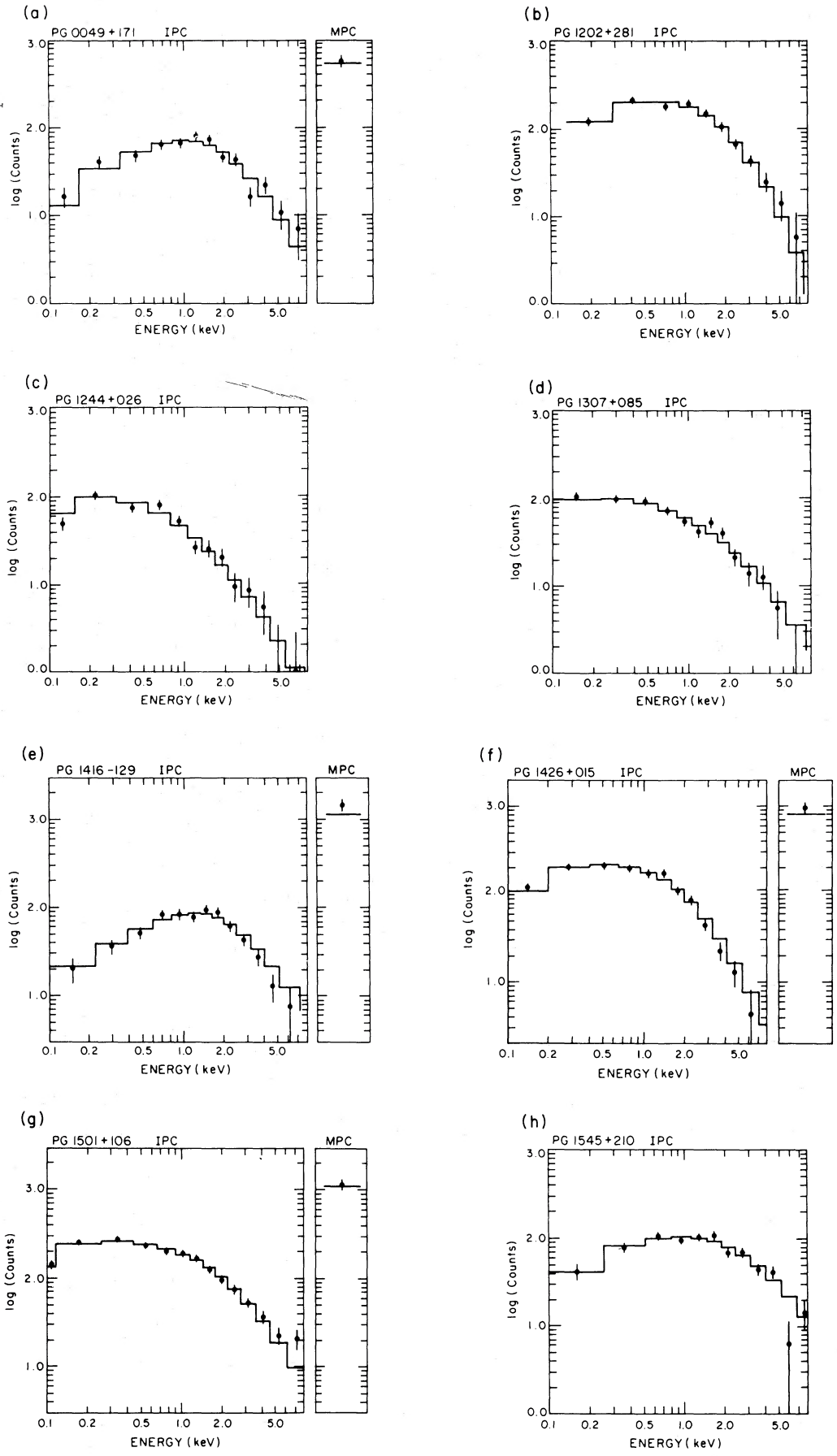

FIG. 2.—Best-fit power-law models compared with the raw IPC and MPC data. Error bars are 1 σ.

TABLE 5

DERIVED QUASAR FLUXES AND LUMINOSITIES FOR POWER-LAW FITS

PG	NAME	f(0.2 keV) (μJy) Intrinsic	f(0.2 keV) (μJy) Observed	f(1 keV) (μJy)	f(2 keV) (μJy) Intrinsic	f(2 keV) (μJy) Observed	f(0.3–3.5 keV) (10^{-11} ergs cm^{-2} s^{-1}) Intrinsic	f(0.3–3.5 keV) (10^{-11} ergs cm^{-2} s^{-1}) Observed	L_x (0.3–3.5 keV) (10^{44} ergs s^{-1}) Intrinsic	L_x (0.3–3.5 keV) (10^{44} ergs s^{-1}) Observed
0049+171[a]....	Mrk 1148	$9.89^{+6.7}_{-6.5}$	$0.02^{+0.32}_{-0.02}$	2.4 ± 0.6	$1.26^{+0.07}_{-0.26}$	$1.22^{+0.08}_{-0.26}$	$1.43^{+0.46}_{-0.27}$	$1.09^{+0.5}_{-0.4}$	$2.7^{+0.9}_{-0.5}$	$2.0^{+0.1}_{-0.7}$
1202+281[a]....	GQ Comae	$7.14^{+5.61}_{-4.21}$	$1.08^{+0.64}_{-0.44}$	$1.21^{+0.13}_{-0.18}$	$0.56^{+0.10}_{-0.06}$	$0.56^{+0.09}_{-0.06}$	$0.72^{+0.10}_{-0.08}$	$0.64^{+0.22}_{-0.03}$	$9.8^{+1.4}_{-1.1}$	$8.74^{+3.0}_{-0.4}$
1244+026	...	$8.6^{+12.6}_{-1.5}$	$4.6^{+0.2}_{-4.1}$	$0.82^{+0.65}_{-0.04}$	$0.3^{+0.20}_{-0.02}$	$0.30^{+0.16}_{-0.10}$	$0.5^{+4.50}_{-0.03}$	$0.5^{+2.40}_{-0.03}$	$0.5^{+0.50}_{-0.03}$	$0.5^{+0.30}_{-0.3}$
1307+085[a]....	...	$5.6^{+6.6}_{-0.8}$	$2.4^{+0.1}_{-0.6}$	$0.87^{+0.09}_{-0.04}$	0.4 ± 0.1	0.4 ± 0.1	$0.52^{+0.07}_{-0.00}$	$0.50^{+0.40}_{-0.02}$	$6.2^{+0.8}_{-0.3}$	$6.0^{+4.7}_{-0.3}$
1416−129[a]....	...	10^{+57}_{-7}	$0.28^{+40}_{-0.28} \times 10^{-3}$	$2.1^{+1.8}_{-0.6}$	$1.08^{+0.07}_{-0.04}$	$1.03^{+0.07}_{-0.04}$	$1.25^{+1.38}_{-0.28}$	$0.83^{+0.04}_{-0.04}$	$10.1^{+11.1}_{-2.3}$	$6.7^{+0.32}_{-0.27}$
1426+015[a,b]...	Mrk 1383	30^{+15}_{-17}	$1.69^{+1.68}_{-0.66}$	3.5 ± 0.4	$1.23^{+0.15}_{-0.10}$	$1.21^{+16}_{-0.10}$	1.9 ± 0.3	1.6 ± 0.1	6.5 ± 1.0	5.5 ± 0.3
1501+106[a,b]...	Mrk 841	22^{+9}_{-2}	$8.0^{+0.2}_{-1.8}$	4.25 ± 0.13	$2.08^{+0.21}_{-0.13}$	$2.07^{+0.21}_{-0.23}$	$2.5^{+0.21}_{-0.06}$	$2.4^{+0.12}_{-0.06}$	$1.4^{+0.20}_{-0.03}$	$1.4^{+0.11}_{-0.03}$
1545+210[b,c]...	3C 323.1	$3.2^{+6.72}_{-1.55}$	$0.49^{+0.08}_{-0.39}$	$1.03^{+0.28}_{-0.10}$	$0.64^{+0.09}_{-0.10}$	$0.63^{+0.11}_{-0.09}$	$0.63^{+1.54}_{-0.06}$	$0.59^{+0.03}_{-0.02}$	$24.5^{+60.0}_{-2.2}$	$23.0^{+1.2}_{-0.9}$

NOTE.—Intrinsic spectra corrected for effects of Galactic absorption by the fit values of Table 4.

[a] Joint IPC/MPC fit values used.

[b] The constraint that N_H be greater than the minimum galactic N_H was used.

[c] The fit to sum of 2054, 2055 was used.

228 Å helium edge. Although in principle the IPC has response at 0.1 keV (124 Å), the uncertainties involved in correcting for the Galactic absorption become absurd. Already at 0.2 keV they are large, as can be seen from Table 5, so we do not quote fluxes below this energy.

b) Ultraviolet, Optical, and Infrared Observations

Ultraviolet spectra were either observed by the authors (PG) or retrieved from the archives of the *International Ultraviolet Explorer* satellite Boggess *et al.* 1978*a*, *b*). A log of the observations is given in Table 6. The targets were observed by blind offset into the large (10″ × 20″) apertures. The spectra were extracted from the line-by-line images produced from the geometrically and photometrically corrected frames by the *IUE* SIPS procedures (Turnrose and Perry 1977), using a five line wide extraction slit for the spectrum, and subtracting a pair of 15 line wide, unsmoothed background swaths. The absolute calibration is from Bohlin *et al.* (1980), with a quoted accuracy of 10%.

Optical spectrophotometry was obtained with the multichannel spectrophotometer (Oke 1969) on the Hale 5 m telescope. The observations were made through 15″ apertures, with decker settings allowing 80 Å bandpasses for wavelengths from 3200 to 5700 Å and 160 Å from 5700 Å to 1.1 μm. Absolute fluxes were calibrated using a flux standard sdG star on the AB79 system (Oke and Gunn 1983) and standard extinction corrections appropriate for Palomar were applied.

Infrared measurements were obtained at the Palomar 5 m telescope. An InSb detector was used for measurements between 1.3 and 3.7 μm. For 10 μm measurements a bolometer system was employed. All the infrared measurements were made through a 5″ aperture with a 15″ north-south chop. Magnitudes were measured relative to standard stars chosen from the lists of Elias *et al.* (1982) and were converted to flux densities using the Caltech system. At 3.7 and 10 μm the filters are sufficiently broad that a color correction should be applied to the flux densities. We made a color correction assuming a Rayleigh-Jeans form for the standard stars and a flux density decreasing linearly with frequency for the objects. This gave a 4% correction at 10 μm and a smaller correction at 3.7 μm. For the 1.2 to 2.2 μm region the color corrections were negligible. Measurement uncertainties are less than 5% from 1.2 to 2.2 μm, ~10% at 3.7 μm, and ~20% at 10 μm.

In Table 7 we list the log of the values for the continuum fluxes in ergs cm^{-2} s^{-1} Hz^{-1} both as observed (col. [2]) and as corrected for reddening and nonsimultaneity of observations (col. [3]), as described below. The 1 σ uncertainty on the values in column (3) are given in column (4). The spectra have been converted to the rest frame of each quasar, using the relations

$$\nu_0 = \nu_{\rm OBS}(1 + z)$$

and

$$f\nu_0 = f_\nu({\rm OBS})/(1 + z)\,,$$

where the values of z are given in Table 1. Column (1) gives log ν_0(Hz). Errors on log f_ν are given in column (4). Data within 10,000 km s^{-1} of strong emission lines—Lyα, Si IV–O IV, C IV, He II, C III, Mg II, Hβ, and Hα—have been deleted.

TABLE 6

IUE OBSERVATIONS

PG	NAME	$E(B-V)$ Nominal	$E(B-V)$ Adopted	LWR IMAGE No.	LWR IMAGE Exposure Time (minutes)	SWP IMAGE No.	SWP IMAGE Exposure Time (minutes)	SHIFT IN log f_{ν_0}
0049+171.....	Mrk 1148	0.058	0.029	...	...	...	...	0
1202+281.....	GQ Comae	0.073	0.036	15078	120	8900	205	−.158[a]
1244+026.....	...	0.058	0.029	15213	120	19223	380	0
1307+085.....	...	0.035	0.017	2826	180	8915	180	0
1416−129.....	...	0.150	0.073	16072	130	8916	145	0
1426+015.....	Mrk 1383	0.081	0.040	15201	80	19214	18	+0.11
1501+106.....	Mrk 841	0.081	0.081	15200	90	19213	180	+0.32
1545+210.....	3C 323.1	0050	0.050	16665	336	20764	428	0

[a] LWR only. No shift for SWP.

TABLE 7

ULTRAVIOLET, OPTICAL, AND INFRARED FLUX DENSITIES

log ν_0(Hz) (1)	log f_ν Values Observed (2)	log f_ν Values Corrected (3)	Errors log f_ν (4)
A. PG 0049+171			
14.9960	-26.17	-26.11	
14.9860	-26.07	-26.01	
14.9750	-26.00	-25.94	
14.9650	-25.98	-25.92	
14.9550	-26.01	-25.95	
14.9450	-25.96	-25.91	
14.9360	-25.99	-25.93	
14.9170	-25.95	-25.90	
14.9090	-25.95	-25.90	
14.9000	-26.00	-25.95	
14.8750	-26.04	-25.99	
14.8590	-26.06	-26.01	
14.8510	-26.09	-26.04	
14.8280	-26.03	-25.98	
14.8140	-26.04	-25.99	
14.8070	-25.99	-25.94	
14.8000	-25.99	-25.94	
14.7730	-25.96	-25.91	
14.7670	-25.99	-25.95	
14.7420	-25.95	-25.91	
14.7380	-26.04	-26.00	
14.7260	-25.98	-25.94	
14.6920	-25.89	-25.85	
14.6820	-25.87	-25.83	
14.6420	-25.81	-25.77	
14.6320	-25.79	-25.76	
14.6230	-25.78	-25.74	
14.6140	-25.73	-25.69	
14.6050	-25.82	-25.78	
14.5970	-25.78	-25.75	
14.5880	-25.73	-25.69	
14.4000	-25.61	-25.58	-26.35
14.2870	-25.47	-25.44	-26.53
14.1580	-25.34	-25.31	-26.58
B. PG 1202+281 (GQ Com)			
15.4256	-26.52	-26.39	-27.26
15.4067	-26.37	-26.24	-27.04
15.3628	-26.37	-26.25	-26.91
15.3546	-26.37	-26.25	-27.08
15.3464	-26.37	-26.25	-26.86
15.3154	-26.54	-26.43	-26.97
15.3080	-26.44	-26.33	-27.01
15.2444	-26.19	-26.22	-26.86
15.2319	-26.17	-26.19	-26.68
15.2197	-26.05	-26.07	-26.68
15.1907	-26.04	-26.06	-26.83
15.1687	-26.06	-26.09	-26.81
15.1582	-26.07	-26.12	-26.96
15.1479	-26.02	-26.07	-27.04
15.1378	-26.06	-26.11	-27.03
15.1280	-26.07	-26.13	-27.21
15.1184	-25.98	-26.05	-27.11
15.1089	-25.99	-26.05	-27.16
15.0997	-25.96	-26.03	-26.79
15.0907	-25.97	-26.04	-27.04
15.0819	-25.93	-26.01	-27.07
15.0732	-25.92	-26.00	-26.93
PG 1202+281—*Continued*			
15.0647	-26.03	-26.10	-26.82
15.0564	-25.95	-26.03	-26.79
15.0482	-26.00	-26.08	-26.57
15.0409	-25.88	-25.96	-26.29
15.0095	-26.07	-25.99	-29.15
14.9940	-26.15	-26.08	
14.9850	-26.08	-26.01	
14.9750	-26.05	-25.98	
14.9570	-26.09	-26.02	
14.9480	-26.05	-25.98	
14.9390	-26.01	-25.95	
14.9310	-26.03	-25.97	
14.9220	-26.06	-26.00	
14.9140	-26.05	-25.99	
14.9060	-26.05	-25.99	
14.8980	-26.10	-26.04	
14.8600	-26.16	-26.10	
14.8530	-26.15	-26.09	
14.8320	-26.12	-26.06	
14.8260	-26.11	-26.06	
14.8130	-26.06	-26.00	
14.8060	-26.05	-26.00	
14.8000	-26.10	-26.04	
14.7430	-26.00	-25.95	
14.7320	-26.02	-25.97	
14.7210	-26.05	-26.00	
14.6910	-25.99	-25.94	
14.6810	-25.99	-25.95	
14.6450	-25.95	-25.91	
14.6360	-25.90	-25.86	
14.6280	-25.87	-25.82	
14.4400	-25.71	-25.67	-26.72
14.3260	-25.48	-25.45	-26.60
14.1950	-25.18	-25.15	-26.30
13.9750	-24.78	-24.75	-25.79
13.5390	-24.44	-24.41	-24.67
C. PG 1244+026			
15.3713	-26.50	-26.40	-27.30
15.3628	-26.44	-26.34	-27.44
15.3546	-26.44	-26.34	-27.27
15.3464	-26.47	-26.37	-27.24
15.3385	-26.47	-26.38	-27.26
15.3307	-26.32	-26.23	-27.13
15.3230	-26.41	-26.31	-27.24
15.3154	-26.44	-26.34	-27.25
15.2463	-26.41	-26.32	-26.87
15.2400	-26.42	-26.33	-27.36
15.2337	-26.33	-26.24	-27.52
15.2276	-26.39	-26.30	-27.25
15.2215	-26.37	-26.28	-27.62
15.2155	-26.36	-26.27	-27.33
15.1785	-26.30	-26.19	-26.78
15.1677	-26.07	-25.96	-26.68
15.1546	-26.38	-26.27	-26.78
15.1418	-26.17	-26.06	-26.63
15.1319	-26.10	-26.00	-26.86
15.1222	-26.27	-26.18	-26.69

TABLE 7—*Continued*

log ν_0(Hz) (1)	log f_ν Values Observed (2)	log f_ν Values Corrected (3)	Errors log f_ν (4)
PG 1244+026—*Continued*			
15.1127	-26.15	-26.06	-26.96
15.1034	-26.11	-26.02	-26.83
15.0943	-26.25	-26.17	-26.97
15.0854	-26.22	-26.14	-26.83
15.0766	-26.14	-26.06	-27.24
15.0681	-26.15	-26.08	-27.15
15.0618	-26.10	-26.03	-26.80
15.0577	-26.15	-26.07	-26.75
15.0535	-26.09	-26.02	-27.12
15.0495	-26.14	-26.07	-27.05
15.0454	-26.17	-26.10	-26.84
15.0414	-26.16	-26.09	-27.30
15.0181	-26.10	-26.04	-26.80
15.0144	-25.99	-25.92	-26.60
15.0107	-26.20	-26.14	-26.70
15.0070	-26.11	-26.05	-26.33
15.0033	-25.89	-25.83	-26.29
14.9997	-26.09	-26.03	-26.23
14.9961	-25.93	-25.87	-26.13
14.9900	-25.65	-25.59	
14.9790	-25.80	-25.74	
14.9690	-25.83	-25.77	
14.9580	-25.80	-25.74	
14.9480	-25.89	-25.84	
14.9370	-25.83	-25.77	
14.9290	-25.89	-25.84	
14.9200	-25.84	-25.79	
14.9110	-25.82	-25.77	
14.8930	-25.98	-25.93	
14.8680	-25.88	-25.83	
14.8600	-25.86	-25.81	
14.8520	-25.88	-25.83	
14.8290	-25.86	-25.82	
14.8220	-25.80	-25.76	
14.8070	-25.77	-25.73	
14.8000	-25.80	-25.75	
14.7730	-25.82	-25.77	
14.7670	-25.82	-25.77	
14.7420	-25.77	-25.73	
14.7360	-25.74	-25.69	
14.7310	-25.74	-25.70	
14.7190	-25.78	-25.74	
14.6970	-25.64	-25.60	
14.6860	-25.72	-25.68	
14.6750	-25.68	-25.64	
14.6450	-25.65	-25.61	
14.6350	-25.53	-25.50	
14.6260	-25.63	-25.59	
14.6170	-25.55	-25.51	
14.6080	-25.69	-25.65	
14.5990	-25.58	-25.54	
14.5900	-25.58	-25.54	
14.5820	-25.50	-25.47	
14.3940	-25.54	-25.51	-26.65
14.2800	-25.44	-25.41	-26.50
14.1490	-25.29	-25.26	-26.46
D. PG 1307+085			
15.4161	-26.01	-25.95	-27.18
15.4067	-25.93	-25.87	-26.79
15.3628	-25.93	-25.88	-27.34
15.3546	-25.90	-25.85	-26.96
15.3464	-25.91	-25.86	-26.83
15.3154	-25.98	-25.93	-26.89
15.3080	-25.95	-25.90	-27.09
15.2468	-25.93	-25.88	-27.43
15.2313	-25.90	-25.84	-26.30
15.2251	-25.88	-25.82	-26.30
15.2191	-25.86	-25.80	-26.55
15.2131	-25.97	-25.90	-26.56
15.1845	-25.86	-25.79	-26.48
15.1790	-25.94	-25.88	-26.46
15.1736	-25.85	-25.79	-26.52
15.1682	-25.92	-25.86	-26.50
15.1629	-25.88	-25.83	-26.57
15.1577	-25.86	-25.81	-26.74
15.1525	-25.86	-25.81	-26.65
15.1474	-25.87	-25.81	-26.65
15.1423	-25.88	-25.83	-26.94
15.1373	-25.86	-25.81	-26.85
15.1324	-25.87	-25.82	-27.00
15.1275	-25.89	-25.84	-26.93
15.1227	-25.84	-25.79	-26.81
15.1179	-25.80	-25.75	-27.10
15.1132	-25.83	-25.78	-27.27
15.1085	-25.82	-25.78	-27.17
15.1039	-25.78	-25.74	-27.01
15.0993	-25.78	-25.74	-27.11
15.0948	-25.74	-25.70	-26.85
15.0903	-25.77	-25.73	-27.05
15.0858	-25.77	-25.73	-26.94
15.0815	-25.76	-25.72	-26.99
15.0771	-25.76	-25.72	-26.87
15.0728	-25.80	-25.76	-26.90
15.0085	-25.79	-25.75	-26.90
15.0643	-25.78	-25.74	-27.05
15.0601	-25.74	-25.70	-26.79
15.0560	-25.77	-25.73	-26.18
15.0519	-25.75	-25.71	-26.39
15.0478	-25.79	-25.75	-27.07
15.0438	-25.73	-25.69	-26.80
15.0398	-25.69	-25.65	-26.42
15.0361	-25.71	-25.67	-26.51
15.0010	-25.65	-25.61	
14.9910	-25.66	-25.63	
14.9810	-25.60	-25.56	
14.9720	-25.64	-25.61	
14.9620	-25.60	-25.57	
14.9530	-25.64	-25.61	
14.9440	-25.60	-25.57	
14.9350	-25.64	-25.61	
14.9270	-25.63	-25.60	
14.9190	-25.62	-25.59	
14.9100	-25.61	-25.58	
14.9020	-25.66	-25.63	
14.8940	-25.66	-25.63	
14.8710	-25.72	-25.69	
14.8570	-25.74	-25.71	
14.8500	-25.70	-25.67	
14.8290	-25.69	-25.66	

TABLE 7—*Continued*

log ν_0(Hz) (1)	log f_ν Values Observed (2)	log f_ν Values Corrected (3)	Errors log f_ν (4)
PG 1307+085—*Continued*			
14.8220	-25.70	-25.68	
14.8090	-25.66	-25.64	
14.8030	-25.70	-25.67	
14.7730	-25.62	-25.60	
14.7390	-25.69	-25.67	
14.7280	-25.71	-25.68	
14.7180	-25.68	-25.66	
14.6970	-25.66	-25.64	
14.6870	-25.66	-25.64	
14.6780	-25.59	-25.57	
14.6410	-25.66	-25.64	
14.6320	-25.57	-25.55	
14.6240	-25.58	-25.56	
14.4360	-25.52	-25.50	-26.53
14.3220	-25.45	-25.43	-26.56
14.1910	-25.28	-25.26	-26.39
13.9720	-25.08	-25.06	-25.94
13.5350	-24.68	-24.66	-24.91
E. PG 1416−129			
15.4161	-26.51	-26.24	-26.97
15.4067	-26.41	-26.15	-26.93
15.3628	-26.43	-26.19	-27.33
15.3546	-26.34	-26.10	-27.10
15.3464	-26.45	-26.21	-26.97
15.3154	-26.65	-26.42	-26.99
15.3080	-26.41	-26.18	-26.77
15.2467	-26.35	-26.11	-27.09
15.0110	-25.74	-25.59	
15.0010	-25.80	-25.65	
14.9910	-25.90	-25.75	
14.9810	-25.84	-25.70	
14.9710	-25.82	-25.69	
14.9620	-25.77	-25.63	
14.9520	-25.81	-25.68	
14.9430	-25.82	-25.69	
14.9340	-25.79	-25.66	
14.9260	-25.80	-25.67	
14.9170	-25.77	-25.64	
14.9090	-25.74	-25.61	
14.9000	-25.78	-25.65	
14.8920	-25.80	-25.67	
14.8690	-25.83	-25.71	
14.8540	-25.91	-25.79	
14.8330	-25.82	-25.70	
14.8260	-25.80	-25.68	
14.8120	-25.81	-25.70	
14.8060	-25.83	-25.72	
14.7990	-25.80	-25.69	
14.7680	-25.80	-25.69	
14.7400	-25.82	-25.72	
14.7290	-25.78	-25.68	
14.7180	-25.76	-25.66	
14.6970	-25.75	-25.65	
14.6870	-25.72	-25.62	
14.6770	-25.68	-25.59	
14.6400	-25.65	-25.56	
14.6310	-25.69	-25.59	
14.6220	-25.69	-25.60	
14.6140	-25.68	-25.58	
14.4260	-25.64	-25.56	
14.3120	-25.59	-25.51	
14.1820	-25.34	-25.27	

log ν_0(Hz) (1)	log f_ν Values Observed (2)	log f_ν Values Corrected (3)	Errors log f_ν (4)
F. PG 1426+015 (Mrk 1383)			
15.4114	-25.43	-25.39	-26.00
15.3587	-25.42	-25.39	-25.75
15.3154	-25.35	-25.33	-25.79
15.2431	-25.39	-25.37	-26.15
15.2306	-25.32	-25.30	-26.12
15.2196	-25.63	-25.60	-25.92
15.0005	-25.32	-25.23	-25.82
14.9840	-25.40	-25.32	
14.9740	-25.38	-25.30	
14.9640	-25.41	-25.33	
14.9540	-25.41	-25.33	
14.9450	-25.40	-25.32	
14.9350	-25.41	-25.33	
14.9260	-25.45	-25.37	
14.9090	-25.43	-25.36	
14.9000	-25.43	-25.36	
14.8920	-25.43	-25.36	
14.8600	-25.49	-25.42	
14.8520	-25.51	-25.44	
14.8300	-25.45	-25.39	
14.8230	-25.44	-25.37	
14.8090	-25.39	-25.33	
14.8020	-25.41	-25.35	
14.7690	-25.43	-25.37	
14.7470	-25.48	-25.42	
14.7350	-25.46	-25.40	
14.7230	-25.42	-25.36	
14.6910	-25.36	-25.30	
14.6800	-25.34	-25.28	
14.6410	-25.31	-25.26	
14.6320	-25.26	-25.21	
14.6230	-25.35	-25.30	
14.6140	-25.29	-25.24	
14.6060	-25.27	-25.22	
14.5970	-25.25	-25.20	
14.4090	-25.21	-25.17	-26.22
14.2950	-25.03	-24.99	-26.15
14.1650	-24.81	-24.78	-25.93
13.9450	-24.62	-24.59	-25.59
13.5090	-24.04	-24.01	-24.76
G. PG 1501+106 (Mrk 841)			
15.4114	-25.26	-24.61	-25.58
15.3628	-25.65	-25.05	-26.91
15.3546	-25.70	-25.10	-26.98
15.3464	-25.68	-25.08	-26.84
15.3154	-25.68	-25.09	-26.57
15.3080	-25.65	-25.07	-26.55
15.2400	-25.70	-25.13	-26.14
15.2337	-25.60	-25.03	-26.91
15.2276	-25.62	-25.04	-26.95
15.2215	-25.61	-25.03	-26.94
15.2155	-25.58	-25.00	-26.85
15.2096	-25.59	-25.00	-26.89
15.1924	-25.58	-24.98	-26.09
15.1867	-25.74	-25.13	-26.47
15.1812	-25.71	-25.10	-26.22
15.1758	-25.69	-25.06	-26.70
15.1704	-25.65	-25.02	-26.48
15.1650	-25.64	-25.01	-26.40
15.1598	-25.62	-24.98	-26.36
15.1546	-25.65	-25.02	-26.45
15.1494	-25.60	-24.97	-26.40

TABLE 7—*Continued*

log ν_0(Hz) (1)	log f_ν Values Observed (2)	log f_ν Values Corrected (3)	Errors log f_ν (4)
PG 1501+106—*Continued*			
15.1443	-25.70	-25.07	-26.44
15.1391	-25.69	-25.07	-26.41
15.1344	-25.68	-25.06	-26.68
15.1295	-25.69	-25.08	-26.78
15.1246	-25.68	-25.08	-26.62
15.1198	-25.61	-25.02	-26.51
15.1151	-25.63	-25.05	-26.41
15.1104	-25.57	-25.00	-26.67
15.1057	-25.57	-25.00	-26.53
15.1011	-25.49	-24.93	-26.54
15.0966	-25.55	-24.99	-26.75
15.0921	-25.56	-25.00	-26.82
15.0876	-25.51	-24.96	-26.53
15.0832	-25.47	-24.92	-26.49
15.0788	-25.47	-24.93	-26.52
15.0745	-25.45	-24.92	-26.47
15.0702	-25.43	-24.89	-26.83
15.0660	-25.47	-24.94	-26.82
15.0618	-25.49	-24.96	-26.76
15.0577	-25.45	-24.93	-26.76
15.0535	-25.47	-24.95	-26.88
15.0495	-25.50	-24.98	-26.59
15.0454	-25.47	-24.95	-26.64
15.0414	-25.45	-24.94	-26.59
15.0181	-25.41	-24.91	-26.59
15.0144	-25.39	-24.89	-26.55
15.0107	-25.44	-24.94	-26.78
15.0070	-25.42	-24.92	-26.38
15.0033	-25.38	-24.88	-26.37
14.9997	-25.43	-24.93	-26.18
14.9961	-25.33	-24.83	-26.05
14.9925	-25.40	-24.91	-26.22
14.9889	-25.46	-24.97	-25.96
14.9850	-25.10	-24.93	
14.9740	-25.08	-24.91	
14.9640	-25.11	-24.95	
14.9530	-25.13	-24.97	
14.9430	-25.10	-24.94	
14.9340	-25.11	-24.95	
14.9240	-25.13	-24.98	
14.9150	-25.14	-24.99	
14.9060	-25.12	-24.97	
14.8970	-25.17	-25.02	
14.8710	-25.18	-25.04	
14.8550	-25.22	-25.08	
14.8320	-25.16	-25.03	
14.8240	-25.16	-25.03	
14.8090	-25.13	-25.01	
14.8020	-25.15	-25.02	
14.7680	-25.16	-25.03	
14.7430	-25.14	-25.02	
14.7370	-25.17	-25.05	
14.7310	-25.15	-25.04	
14.7260	-25.18	-25.07	
14.6920	-25.08	-24.96	
14.6810	-25.07	-24.96	
14.6400	-25.05	-24.94	
14.6300	-25.02	-24.92	
14.6210	-25.03	-24.93	
14.6120	-24.99	-24.88	
14.6030	-25.01	-24.90	
14.5940	-25.00	-24.90	
14.5850	-24.99	-24.89	
14.5770	-24.99	-24.89	
14.3890	-24.96	-24.88	-26.08
14.2750	-24.82	-24.74	-25.93
14.1440	-24.66	-24.59	-25.68
13.9240	-24.44	-24.37	-25.21
H. PG 1545+210 (3C 323.1)			
15.4768	-26.49	-26.30	-26.91
15.4609	-26.44	-26.26	-27.11
15.4404	-26.55	-26.37	-27.14
15.4209	-26.52	-26.36	-27.05
15.3713	-26.61	-26.45	-26.91
15.3628	-26.46	-26.30	-27.02
15.3546	-26.31	-26.16	-26.65
15.3464	-26.44	-26.29	-27.02
15.3385	-26.32	-26.17	-26.94
15.2727	-26.33	-26.15	-27.04
15.2626	-26.25	-26.07	-27.01
15.2495	-26.40	-26.20	-26.93
15.2368	-26.14	-25.95	-26.43
15.2245	-26.28	-26.10	-26.93
15.2125	-26.36	-26.19	-27.04
15.2009	-26.25	-26.08	-27.09
15.1895	-26.21	-26.06	-27.12
15.1785	-26.29	-26.15	-27.14
15.1677	-26.24	-26.10	-27.12
15.1572	-26.19	-26.06	-27.18
15.1468	-26.18	-26.05	-27.27
15.1368	-26.22	-26.10	-27.20
15.1270	-26.19	-26.07	-27.41
15.1174	-26.12	-26.01	-27.14
15.1080	-26.05	-25.94	-27.08
15.0988	-26.10	-25.99	-27.00
15.0817	-25.97	-25.86	-27.27
15.0710	-25.88	-25.77	
15.0600	-25.90	-25.79	
15.0500	-25.90	-25.80	
15.0110	-25.88	-25.79	
15.0010	-25.88	-25.79	
14.9920	-25.88	-25.79	
14.9750	-25.84	-25.75	
14.9660	-25.84	-25.76	
14.9580	-25.84	-25.75	
14.9490	-25.84	-25.75	
14.9410	-25.83	-25.75	
14.9330	-25.83	-25.74	
14.9260	-25.83	-25.75	
14.9180	-25.83	-25.75	
14.9100	-25.85	-25.76	
14.9030	-25.83	-25.75	
14.8960	-25.85	-25.77	
14.8750	-25.88	-25.80	
14.8550	-25.88	-25.80	
14.8480	-25.87	-25.80	
14.8290	-25.86	-25.79	
14.8230	-25.86	-25.79	
14.8120	-25.93	-25.85	
14.8010	-25.87	-25.80	
14.7670	-25.85	-25.78	
14.7460	-25.86	-25.79	
14.7360	-25.84	-25.77	
14.7260	-25.84	-25.77	
14.7170	-25.82	-25.76	
14.6980	-25.77	-25.71	
14.6890	-25.77	-25.71	
14.6800	-25.81	-25.75	
14.4750	-25.76	-25.71	-26.88
14.3610	-25.63	-25.58	-26.75
14.2310	-25.48	-25.44	-26.60

A power-law slope was calculated for the 1–10 μm data and was used to predict a flux density at 1 keV by a simple extrapolation. These quantities are given in Table 8, where they are compared with the X-ray slope and observed 1 keV flux. We had too little infrared data to define a slope for PG 1416−129. Ward *et al.* (1986) show that 10 μm fluxes in Seyfert galaxies (among which they include PG 1501+106 [Mrk 841]) may be dominated by dust emission associated with the forbidden line region. We have thus repeated the slope calculation without the 10 μm points and find no substantial difference in the derived values.

c) *Variability and Reddening*

One difficulty with relating the spectrophotometry from different instruments is the nonsimultaneity of the observations. Table 1 shows that most observations took place during 1980–1981. These optically selected quasars typically vary by only $\sim$0.1 mag at B (W. Keel, private communication) and by less than 0.2 mag at K (as seen from repeated infrared observations collected for this study). On such time scales, optical variability should not be a major problem. However, three of the *IUE* observations taken in 1983 showed discontinuities with the earlier optical data. We therefore grayshifted the *IUE* images (by adding the $\Delta \log f_\nu$ values given in Table 6 to all the *IUE* continuum fluxes in Table 7, col. [2]), to match the multichannel data. Factors of 1.3, 0.7, and 2.1 are involved. We note that studies of Seyfert and quasar spectral variability have shown that the continuum generally varies more toward the ultraviolet, giving a flatter f_ν slope as the luminosity increases (Cutri *et al.* 1985), so that a grayshift may not be appropriate.

Only one of our eight quasars is a confirmed optical variable, PG 1202+281 (GQ Comae). In the interval between 1979 May and 1980 November it varied by only 0.4 mag, with $m_{pg} = 15.8$–16.2 (Barbieri, Cristiani, and Romano 1982). This interval spans all the observations except the *IUE* LWR data which were taken in 1983 January. Near this time, in 1983 April, M. Sitko (private communication) found PG 1202+281 to be in a high state in the optical and ultraviolet. It is not surprising, then, that we had to reduce the LWR flux points to match the earlier data smoothly.

There is also an uncertainty introduced by the nonsimultaneity of the X-ray observations and the observations in the other bands. PG 1426+015 was noted as a variable X-ray source by Zamorani *et al.* (1984), who saw a 50% change in 6 months. Arnaud *et al.* (1985) find 12% variations in one day in PG 1501+106. Our observation of this quasar, taken $4\frac{1}{2}$ yr earlier, has a 1 keV flux density $\sim$25% higher than that of Arnaud *et al.* These in themselves are not major effects. However, we have no way of estimating other possible variations in the X-rays. None of the conclusions of § III are particularly sensitive to uncertainties in correcting for variability at low levels (a factor of 3 or less).

Finally, we made corrections for the effect of interstellar reddening. Small uncertainties in $E(B-V)$ can lead to large uncertainties in the ultraviolet flux. Also, in principle, dust located in the quasar can further redden the intrinsic spectrum, with a reddening law different from the average Galactic curve. We can estimate the reddening in several ways. The galactic N_H values (Stark *et al.* 1985) and the assumption that $N_H/E(B-V) = 4.8 \times 10^{21}$ atoms cm^{-2} mag^{-1} (Bohlin 1978) imply the "nominal" $E(B-V)$ values in Table 6. The X-ray spectrum constrains the total N_H as in Table 4 and is consistent in all cases with the galactic N_H value. The constraint that the reddening correction not overcompensate for the 2200 Å bump in the reddening curve limits the total $E(B-V)$ slightly more tightly than the Bell Labs' measurements, assuming that any dust along the line of sight has this feature. We will use the "adopted" Galactic $E(B-V)$ values given in Table 7, which come from this constraint on the 2200 Å feature, and correct the fluxes using the reddening curve of Seaton (1979). We note in § III whenever conclusions are sensitive to this choice of $E(B-V)$.

III. DISCUSSION

a) *X-Ray Spectra*

i) *Comparison with Previous X-Ray Data: Selection Effects*

The mean best-fit power-law index for the PG quasars studied here is 1.05, with an observed dispersion of 0.25. Figure 3 summarizes the power-law index results for these eight quasars. These results also suggest that there is no universal X-ray spectrum for PG quasars. Five of the quasars have slopes inconsistent with the "canonical" value of 0.7 at 90% confidence. PG 1244+026 is steeper than 1.0 at better than 90% confidence. The error on the mean of the slopes is 0.05, so that the mean slope is 7 σ steeper than the "canonical" 0.7 value.

Even if a single power law is not a correct description of these quasar spectra and, for example, a two-component fit is a better approximation, this mean value is very different from the 0.7 slope found in other spectral surveys, including those made at low energies (Mushotzky 1984; Petre *et al.* 1984; Pounds 1985). Optically selected quasars seem to have steeper X-ray spectra than hard X-ray selected AGNs. This difference could be due to selection effects or could be a real physical difference. We now examine these possibilities.

We can imagine four reasons:

1. The extra sensitivity of the IPC allows it to see more distant and more luminous quasars. There might be some luminosity, or redshift, dependence of the X-ray spectral index.
2. The low-energy boundary of the IPC is $\sim$0.1 keV, well below the 0.75 keV of the *Einstein* SSS. This might take the IPC into the region where the X-ray continuum turns up to meet the UV continuum, which is typically 100 times the flux density of the hard X-ray continuum and only one and a half decades below in frequency.
3. The ultraviolet excess requirement for inclusion in the PG sample might select objects with anomalously strong "big bumps" (see § III*b*[i]) and which might then be peculiar in their X-ray properties.
4. The AGNs for which the original "canonical" slope was determined were found in the 2–10 keV all-sky surveys (e.g., *HEAO 1* A-2) and are thus selected to be strong *hard* X-ray sources. On the other hand, to have a spectrum measured by the IPC an AGN needs to give at least 500 counts in one observation, biasing our sample toward strong *soft* (0.1–4.0 keV) X-ray sources. Thus, selection effects may be introducing the discrepancy between the two data sets toward flat and steep spectra respectively.

We consider each of these possibilities in turn.

Luminosity effects are probably not important. A comparison of the luminosity ranges of the two samples shows that the current IPC sample has a mean luminosity only a factor of 3 higher than that of the SSS sample (Petre *et al.* 1984) or the *HEAO 1* A-2 sample (Mushotzky 1984; Fig. 4). There is no trend within our data for higher luminosity quasars to have

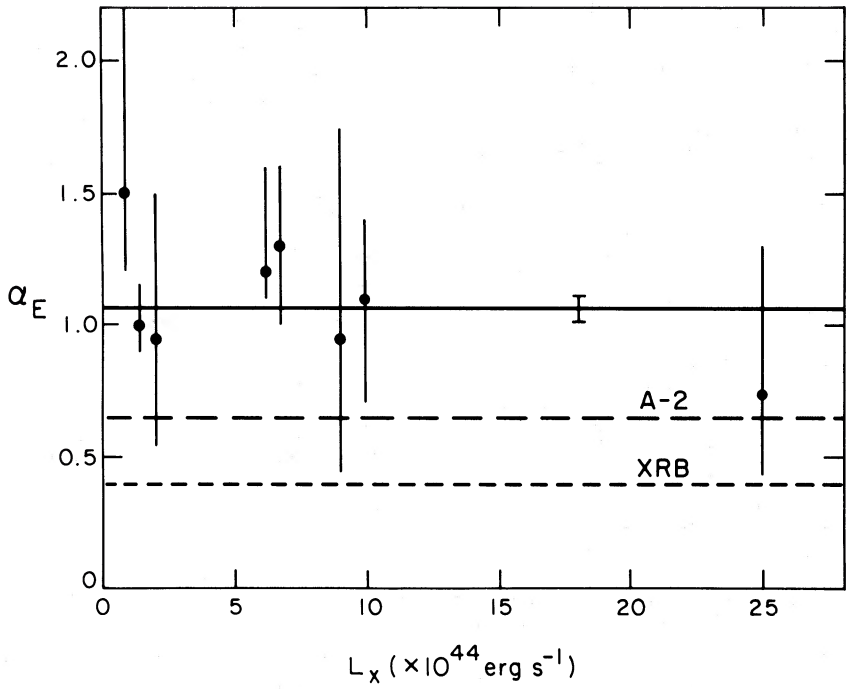

FIG. 3.—Best-fit power-law indices with 90% error bars vs. X-ray luminosity. *Solid line:* mean, with a 1 σ error bar. *Long-dashed line:* mean slope found for the *HEAO 1* A-2 sample. *Short-dashed line:* slope of diffuse X-ray background in the 3–10 keV range.

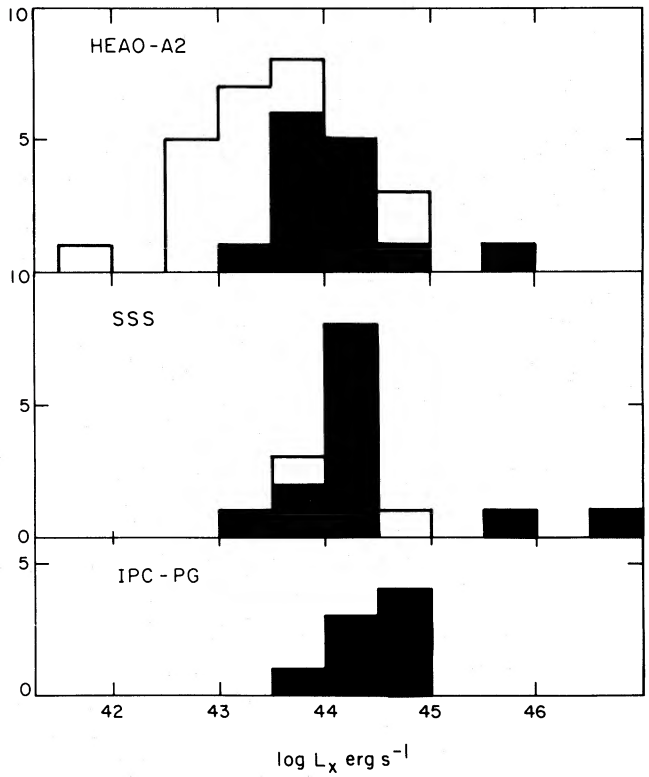

FIG. 4.—Comparison of the luminosities of the eight PG quasars in this paper with the *HEAO 1* A-2 and SSS samples. *Solid areas,* AGNs with measured spectra.

steeper spectra (Fig. 3). However, the luminosity range that we cover is very limited. (Note that Fig. 3 has a *linear* luminosity axis). None of the quasars in our sample has a redshift greater than 0.3, so that any evolutionary effect would have to be very strong to be significant.

The lower energy range of both the IPC and SSS compared to *HEAO 1* A-2 does seem to be important. The IPC and SSS spectral indices for Seyfert galaxies agree to *better than* the quoted SSS errors (Fig. 5). If 0.7 were really a universal slope for these data, we would see a scatter diagram centered on (0.7, 0.7). Instead there is a clear correlation. A comparison of the SSS results with the higher energy *HEAO 1* A-2 data shows no such correlation (see Fig. 4*b* of Petre *et al.* 1984). Two of the six Seyferts (ESO 141−G55, NGC 7469) have a suggestion of soft excess. Even hard X-ray selected galaxies, then, show some diversity in their low-energy spectra. More directly, PG 1211+143 (Elvis, Wilkes, and Tananbaum 1985; Paper II) has a two-component spectrum and the IPC/MPC fit at high energies for PG 1416−129 suggests a similar soft excess.

However, this is probably not the case for all quasars. As noted in § I, soft excesses seem to be relatively rare in hard X-ray selected AGNs (Pounds 1985). An energy range difference alone cannot be the complete explanation. For the other three quasars with MPC data, the higher energy IPC/MPC fits suggest that it is not simply the low IPC energy range that leads to the steeper spectral indices, but that the steeper slopes continue to at least ~6 keV. In particular, the soft excess found by Arnaud *et al.* (1985) is due to a ~0.1 keV *EXOSAT* data point. This soft excess is unlikely to produce a significant effect on the IPC/MPC fit to data above 0.65 keV (see § II*a*[iii]).

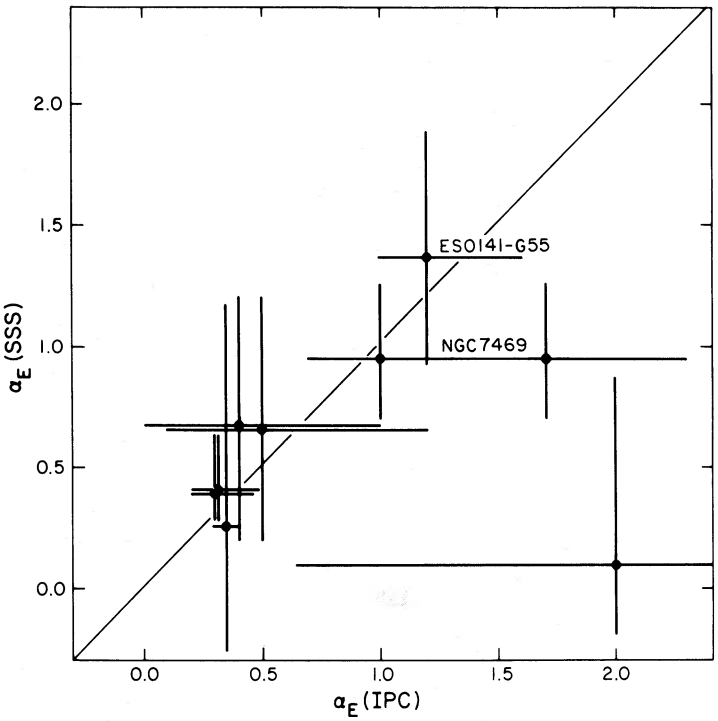

FIG. 5.—Comparison of IPC and SSS slopes for eight emission-line AGNs (Harnden and Fabricant 1985). (Note: these are not PG quasars.)

Possibly, soft excesses are more common in UV-excess selected quasars leading to a bias in the spectral results. The $U-B < -0.44$ criterion for the selection of PG quasars (Schmidt and Green 1983) requires an optical-UV component having a slope flatter than 1.2 in the U and B bands. This is not a particularly extreme requirement, and it would be surprising if it were important. We can show that this is not a major effect by considering the $U-B$ colors of the *HEAO 1* A-2 sample. The PG $U-B$ color criterion would include half (13 of 25) the AGNs with *HEAO 1* A-2 spectra (as summarized in Mushotzky 1984; $U-B$ colors were taken from Véron-Cetty and Véron 1985). These AGNs have similar X-ray luminosities to the PG quasars studied in this paper. The distribution of *HEAO 1* A-2 indices for these "PG-qualified" UV-excess AGNs is identical to that of the *HEAO 1* A-2 sample as a whole with a mean of 0.7. If UV excess alone were the cause of the difference in slopes, we would have found the UV-excess subsample of *HEAO 1* A-2 AGNs to have a distribution of α_E peaked at a steeper index.

Since the PG sample is optically selected and the *HEAO 1* A-2 AGNs are X-ray selected, the PG objects may have larger l_{opt}/l_x ratios or, in the customary notation (Zamorani *et al.* 1981), larger α_{ox} values. Figure 6 compares the α_{ox} distributions of the PG sample (Tananbaum *et al.* 1986) and the Piccinotti sample (Piccinotti *et al* 1982; Cheng *et al.* 1984). Overall the PG sample does indeed have larger α_{ox}. However, the subset for which we have IPC spectra (*shaded*) has essentially the same α_{ox} distribution as the Piccinotti sample (Fig. 6). We would expect to pick out the low-α_{ox} tail of the PG sample in our IPC spectral survey, since these are the objects that give the strongest X-ray fluxes.

A soft X-ray excess should lead to a systematic underestimate of the absorbing N_H column by the IPC. Using the N_H values in Tables 2 and 4 for 21 cm– and IPC–determined column densities respectively gives good agreement between the two. The mean value for N_H (21 cm) $- N_H$ (IPC) is $0.14 \pm 1.34 \times 10^{20}$ atoms cm^{-2} (excluding PG 1416−129, which has large IPC errors in N_H). This is some evidence against a soft excess explanation of the steeper mean α_E of the PG quasars.

So far, then, we have shown that luminosity and redshift effects, as well as the UV selection criterion for PG quasars, can be excluded as the cause of the difference in X-ray slopes between the IPC and *HEAO 1* A-2. The lower energy range of the IPC is relevant in a minority of objects (those with soft exessses) but probably not in all. The remaining possibility is that it is biases in the selection of the samples which cause the difference.

It does not seem surprising that the objects which are brightest in the hard X-ray band should have flat, hard spectra that will give them detectable photon fluxes at $\sim$6 keV. The reduction in expected count rate as a function of steepening the spectral index can be quite crucial in reducing the representation of steep spectrum objects in the sample. The hard X-ray samples are small. (There are 29 emission-line AGNs in the Piccinotti *et al.* 1982 sample.) A small change in the 2–10 keV flux of a population then can leave only a few examples in these surveys. We can suggest the size of the effect as follows. For a constant normalization (i.e., constant 1 keV flux density), a change of spectral index from 0.7 to 1.0 reduces the 2–10 keV count rate by a factor of 1.5. A slightly larger change in the index from 0.65 to 1.2 causes a reduction by a factor of 2.05. If the flat- and steep-spectrum populations have the same luminosity function at 1 keV, then the steep population will be significantly underrepresented in the hard X-ray surveys such as that of Piccinotti *et al.* (1982). Of course, the luminosity functions for the X-ray steep-spectrum and X-ray flat-spectrum quasars need not be the same at 1 keV. From the absence of

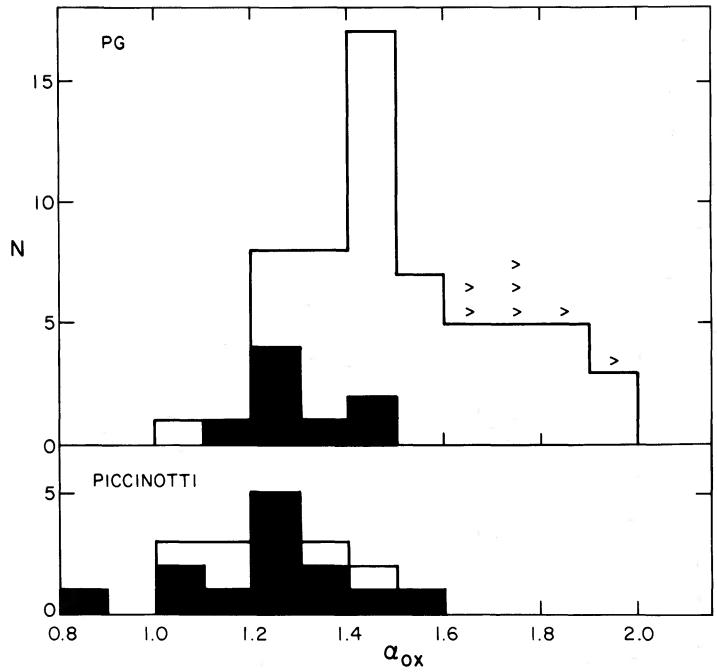

FIG. 6.—Comparison of α_{ox} for the Piccinotti sample (*objects included in shaded region* have measured X-ray spectra), and the PG quasar sample (*objects in shaded region* have X-ray spectra reported in this paper). Arrows are lower limits to α_{ox}.

steep-spectrum objects in the surveys with brighter flux limit, we can say that the (very) local space density of steep spectrum sources cannot exceed that of the flat-spectrum objects by a large factor.

If there is a distribution of spectral indices in the parent quasar population, then the *HEAO 1* A-2 objects represent the flattest segment of that population. The value 0.7 may be an approximate *limit* to the range of α_E rather than a universal value. The test of this selection criterion will be to measure 2–10 keV spectra for samples of quasars selected by other methods. This may be possible in a limited way with an improved MPC analysis or with *EXOSAT* and will certainly be easily done with AXAF.

Our sample of PG quasars is not free from bias either. All the PG quasars were pointed at by *Einstein* for similar exposure times (Tananbaum *et al.* 1986). Most did not give more than a few tens of counts, inadequate for a useful spectral fit. The quasars discussed here are thus abnormally X-ray bright for their optical magnitude. Figure 6 shows this bias in terms of α_{ox}, the nominal spectral slope between 2500 Å and 2 keV. Being selected to have a high count rate in the soft IPC band, these eight quasars might be abnormally steep. The soft X-ray spectra of the high-α_{ox} PG quasars will be measurable with ROSAT but their hard X-ray properties must await AXAF.

In summary, this seems to be a real physical difference between optically selected and hard X-ray selected AGNs even at the same luminosity and optical to X-ray ratio α_{ox}. We do not know whether this difference persists for the whole PG sample, since adequate data do not exist. The cause of this difference is not clear. Soft excesses over a canonical power law might be more common in PG quasars, or their power-law spectra may be intrinsically steeper. The MPC data and the good agreement between the IPC–derived N_H values and those from 21 cm H I surveys suggest that a steeper intrinsic spectrum is the more likely explanation.

ii) *Emission Processes*

If our PG quasar power laws are intrinsically steeper than the canonical value, then the X-ray spectra alone can limit the applicability of some proposed models to PG quasars. The model of Mészáros (1983) integrates the thermal bremsstrahlung emission over the range of temperatures produced in a spherical accretion flow. For maximum temperatures T_{max} greater than ~ 50 keV, the 0.1–10 keV spectrum that is formed is a good approximation to a power law of slope 0.7. A slope of ~ 1.0 is clearly not allowed in this region.

Power-law slopes of 1.0 also do not fit into the simple analogy between Galactic X-ray binaries and AGNs of White, Fabian, and Mushotzky (1984). Black hole candidate X-ray binaries such as Cyg X-1 switch between high and low states. In their low states they have hard 2–10 keV spectra with slopes of ~ 0.7. In their high state they have steep $\alpha \approx 2.5$ slopes. This suggests that accretion onto a black hole has only two available modes that produce two characteristic slopes, with a crossover point between the two states occurring at some fraction (~ 0.02) of the Eddington limit. The two slopes are similar to those of the hard X-ray selected AGNs and of BL Lac objects respectively. The existence of quasars with X-ray spectral slopes of 1.0 (so long as these are not composites of two components) implies that the analogy to Galactic binaries is not so straightforward as proposed by White *et al.* An analogy may yet exist in a more general form (e.g., accretion disk plus power law), but more examples of Galactic black hole binaries will be needed before this claim can be made.

Soft X-ray emission from quasars is expected from the hot gas which is generally thought to be necessary to confine the emission-line clouds (Krolik, McKee, and Tarter 1981; Halpern and Filippenko 1984). Thermal bremsstrahlung fits to the quasar spectra give temperatures of ~ 2.5 keV with a range from 1.0 to 4.5 keV. With this temperature we can derive an emission measure $n_e^2 V$ for each quasar. For typical values of

temperature and density in the different emission-line clouds we can define a density for the hot gas that gives pressure equilibrium and hence find an effective radius. We use PG 1202+281 as an example. It has a best-fit temperature of 2.7 keV and an emission measure of 7×10^{67} cm^{-3}. The emission-line clouds all have temperatures of $\sim 10^4$ K. A low-density ($n_e \approx 10^4$ cm^{-3}) narrow-line region gives a radius of ~ 2 kpc. A more dense narrow-line region ($n_e \approx 10^6$ cm^{-3}) gives a radius of ~ 200 pc. These are rather large values for these regions. A typical broad-line region cloud has $n_e \approx 10^{9.5}$ and yields a radius of ~ 1 pc, comparable to the typical broad-line region size. It is possible then that thermal emission from the broad-line region makes a significant contribution to the X-ray emission from these quasars. Variability on time scales of months or less would rule out such a possibility. Variability has been reported in PG 1426+015 (Zamorani *et al.* 1984) and PG 1501+106 (Arnaud *et al.* 1985). These results suggest that thermal emission does not dominate the X-ray emission of these quasars.

As we have noted, the measured IPC slopes may be an average of two components, at least in some cases, so that data with better energy resolution will be needed to test these possibilities definitively.

iii) *Evolution and the X-Ray Background*

Quasars have been widely discussed as a source population whose integrated emission may constitute the diffuse X-ray background. As such, their summed spectra over redshift and luminosity must match that of the X-ray background. Most of the discussion has concerned UV-excess selected quasars such as the PG sample (Marshall *et al.* 1984; Schmidt and Green 1986; Avni and Tananbaum 1986). In the range 2–10 keV, the background spectrum is close to being a power law of slope 0.4 (Marshall *et al.* 1980). This is clearly not the slope we see with the IPC (Fig. 3). Since our sample of PG quasars is biased in α_{ox} (Fig. 6)[5] and the energy range we cover is mostly in a band below 2 keV, for which the extragalactic X-ray background spectrum is not well known (Nousek *et al.* 1982), this discrepancy of slope does not rule out quasars as the source of the X-ray background.

It does make this possibility less likely, however, for two reasons. First, it would seem to require a distinct break in the typical quasar spectrum just at the top of the IPC energy range. Such a break does not appear to be present in three of the four quasars in our sample with MPC data. Second, the 2 keV flux densities used by most previous authors are *derived* quantities and require a spectral index assumption. For example, changing the assumed index from 0.5, the traditional value, to 1.2 reduces the 2 keV flux by $\sim 40\%$, which in turn reduces the 2 keV background contribution made by these quasars. Schmidt and Green (1986) explore some of the consequences of changing the assumed index.

[5] The quantity α_{ox} is based on an extrapolation of the measured *B*-band flux to 2500 Å using the formula of Schmidt (1968) and Marshall *et al.* (1984). Our UV data allow us to check the reliability of this extrapolation for six quasars. The observed and predicted log f_ν have a scatter of 0.1, but the mean of the six values is -0.02. So for these quasars the Schmidt formula is reliable, on average, to a few percent.

b) Broad-Band Spectra

i) *X-Ray to Infrared Spectra*

Figure 7 presents the entire X-ray to infrared data set for the eight quasars in this study. Rather than the traditional log f_ν versus log ν plots, we have used the less familiar but, we believe, more useful log νf_ν versus log ν plots. Since quasars follow, roughly, an $f_\nu \propto \nu^{-1}$ distribution over a wide range of frequency, it is easier to see deviations from this linearity in a log νf_ν plot.

The most striking feature of the νf_ν plots is the strong rise from the optical toward the EUV. This suggests that the EUV luminosity dominates the bolometric output of these quasars. The second obvious point is the approximate νf_ν = constant distribution of the infrared and X-ray data. In particular we note that, even though these are the smallest α_{ox} objects in the PG sample, there is no case in which the X-rays lie well above the infrared νf_ν value. Such objects would be easily found by *Einstein* observations, and their absence suggests that some limiting process prevents the existence of more X-ray bright objects.

The other clear feature of these plots is the approximate continuity between the infrared (1–10 μm) and the X-ray (0.2–3 keV) continua in both slope and normalization. This suggests that a single mechanism may produce the entire five decades of power-law continuum in some of these quasars and that the X-ray slopes we measure may be truly single component power laws. To quantify this impression of continuity, Figure 8 and Table 8 compare the infrared and X-ray slopes. The data are certainly *consistent* with the idea of a single power law from infrared to X-rays, but the errors are sufficiently large so as not to *demand* such a continuity. Figure 9 and Table 8 also compare the 2 keV flux predicted by extrapolating the infrared slope with that actually observed. There is agreement to within a factor of a few except for PG 1202+281. This is the most variable of the quasars optically, which might explain the poor prediction. Its unusually steep infrared slope also suggests that this quasar might have significant hot dust emission.

TABLE 8

INFRARED SLOPES AND EXTRAPOLATED 1 keV FLUXES COMPARED WITH X-RAY RESULTS

PG	Name	α_E[a]	α_{IR}	f(1 keV) Predicted	f(1 keV) Observed[b]
0049+17	Mrk 1148	$0.95^{+0.6}_{-0.4}$	1.05 ± 0.23	2.02 (0.39–10.4)	2.4 ± 0.6
1202+281.....	GQ Comae	$1.1^{+0.3}_{-0.4}$	1.84 ± 0.12	0.01 (0.004–0.048)	$1.21^{+0.12}_{-0.18}$
1244+026.....	...	$1.5^{+1.3}_{-0.3}$	1.00 ± 0.16	3.05 (0.97–9.57)	$0.82^{+0.65}_{-0.00}$
1307+085.....	...	$1.2^{+0.4}_{-0.1}$	0.97 ± 0.12	3.98 (1.71–9.27)	$0.87^{+0.08}_{-0.00}$
1426+015.....	Mrk 1383	1.3 ± 0.3	1.25 ± 0.075	1.40 (0.82–2.39)	3.5 ± 0.4
1501+106.....	Mrk 841	$1.0^{+0.2}_{-0.05}$	1.09 ± 0.12	7.53 (3.19–17.78)	4.25 ± 0.07
1545+210.....	3C 323.1	$0.75^{+0.55}_{-0.3}$	1.09 ± 0.16	1.34 (0.42–4.27)	$1.03^{+0.28}_{-0.09}$

a From Table 4.

b From Table 5 using fits with $N_H > N_H$(gal, min) and corrected for Galactic absorption.

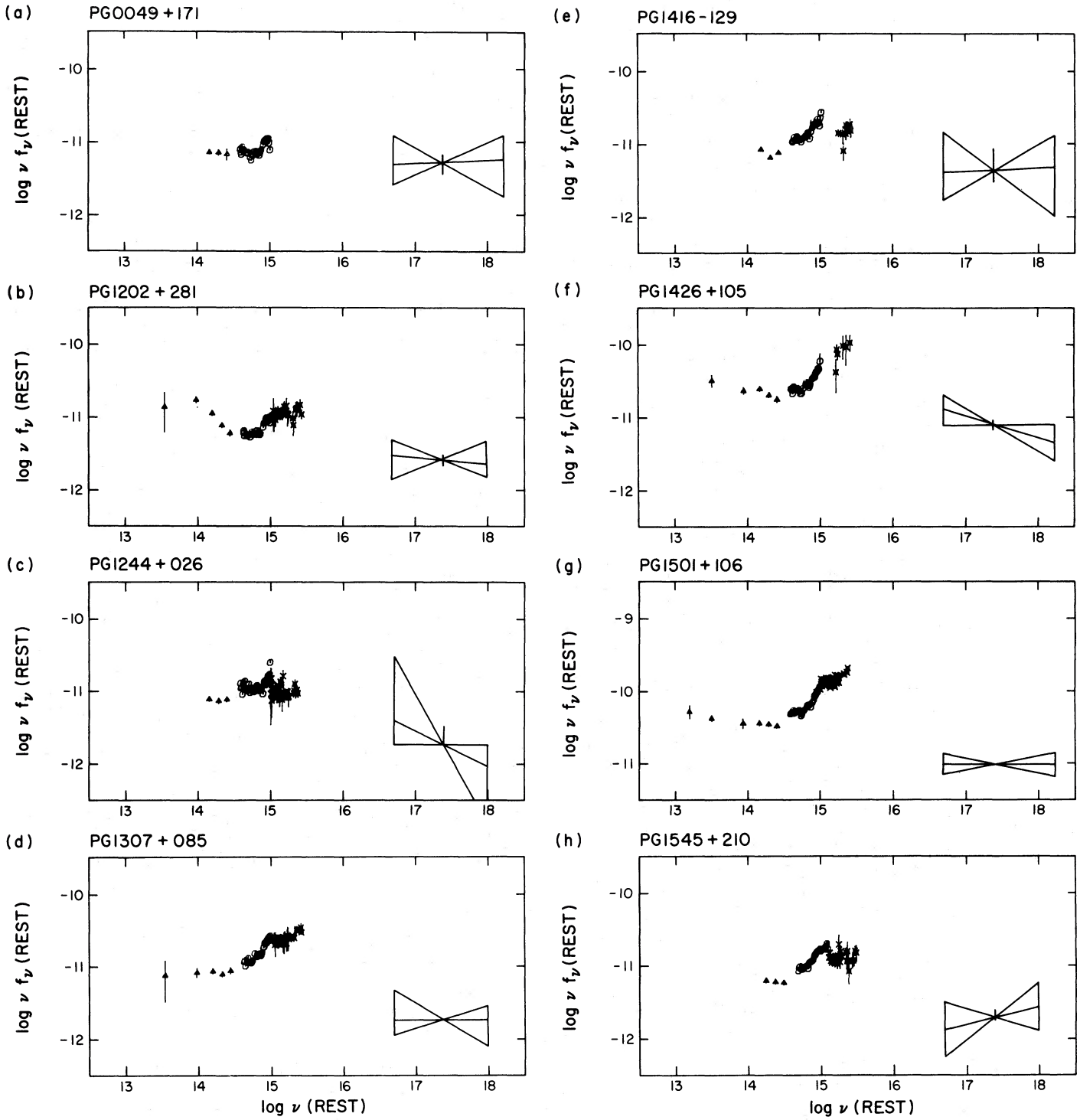

FIG. 7.—X-ray to infrared energy distributions for the eight PG quasars log νf_ν (ergs cm^{-2} s^{-1}) vs. log ν (Hz). The bowtie shape shows the 90% confidence limits on the X-ray slope, the central line being the best fit. For quasars with only IPC data the X-ray fits are shown between 0.2 keV and 4 keV. For quasars which also have MPC data the fit is shown extending to 7 keV. The error on the normalization at 1 keV is shown as a vertical line very close to the crossing point of the bowtie. *Crosses*, *IUE* data; *circles*, optical multi-channel data; *triangles*, infrared photometry points.

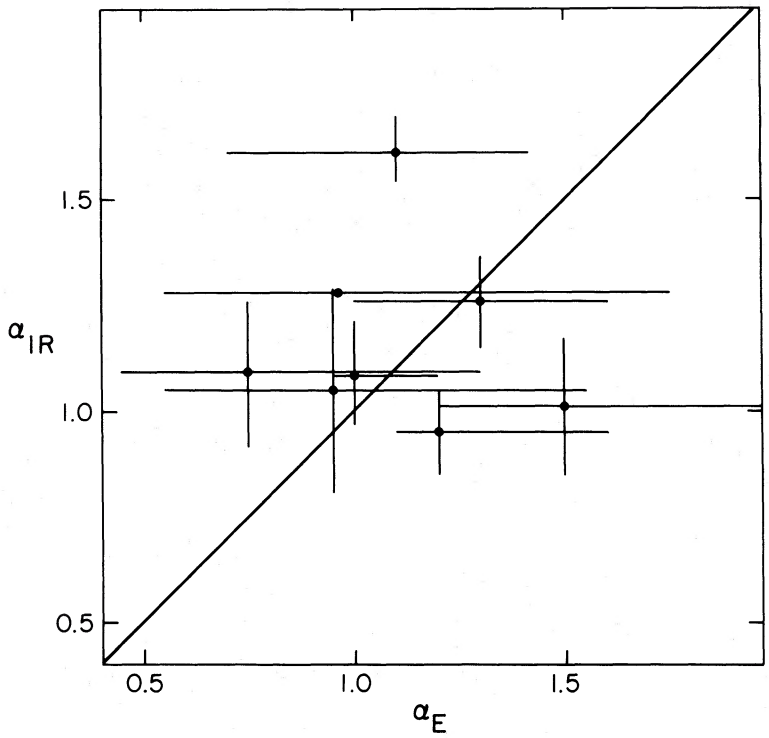

FIG. 8.—Comparison of infrared 2–10 μm (α_{IR}) and IPC/MPC (α_E) slopes. 90% error bars are shown.

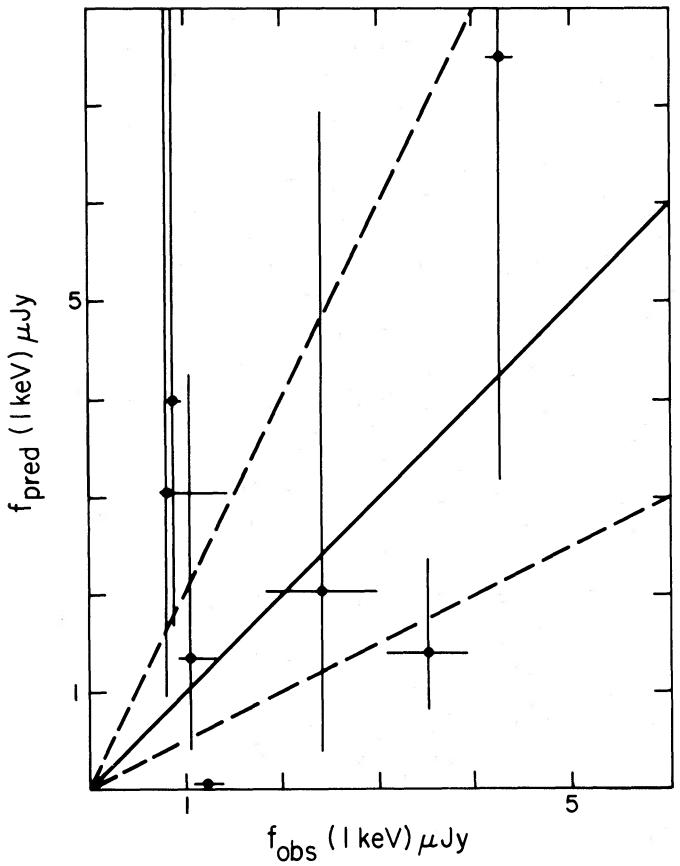

FIG. 9.—Comparison of the observed 1 keV flux with that predicted by extrapolating the infrared slope. The solid diagonal line indicates equality and the dashed lines show factor of 2 uncertainties.

The strong rise in the optical/UV range is seen clearly in six of the eight quasars. This "bump" has been much discussed in the literature (Shields 1978; Richstone and Schmidt 1980; Puetter *et al.* 1982; Malkan and Sargent 1982). There has been some confusion between this bump and the "3000 Å bump" (Grandi 1982). This second feature is also clearly visible in several of our quasars (it is particularly clear in PG 1307+085 and PG 1501+106, Figs. 7*d* and 7*g*). We refer to the "3000 Å bump" as "small bump" and the whole upturn from $\sim$1 μm blueward as "big bump" (following the suggestion of Elvis 1985 and Elvis and Lawrence 1985).

The small bump has been convincingly argued to be a combination of Balmer continuum and a blending of hundreds of broad, permitted Fe II lines by Wills, Netzer, and Wills (1985). The big bump is most often interpreted as the integrated thermal emission from an accretion disk (Shields 1978; Malkan and Sargent 1982; Paper II). The decomposition into a power law with a superposed big bump was previously based on an extrapolation of the infrared continuum alone. The apparent continuity of the infrared and X-ray continua seems to make this two-component decomposition of the spectrum more convincing. The big bump seems to have a range of amplitudes in these quasars. Although uncertainties in the reddening may affect the slope and amplitude of the big bump, the low N_H values derived from the X-ray spectra suggest that this effect should not be large and so cannot explain this range of amplitudes. This variation needs to be addressed in any attempts to model the big bump.

In contrast, the big bump is always seen to depart from the infrared power law around 1 μm, both in our data and in those of Malkan and Sargent (1982). The extremes of its range lie between 0.5 and 1.5 μm. This narrow range suggests some energy balance between the "power-law" 'and big-bump components. Assuming the two components always to have the

same shape, then the "turn-up" point for the big bump will just be a reflection of their relative luminosities. It seems that this ratio is almost constant and is, to order of magnitude, unity. In Paper III we discuss the correlations between these two components and the big bump. The infrared and X-ray continua are clearly linked in some way even if their identification as two ends of a single-component power law proves incorrect. Several models have been made which would connect the two regimes, and we discuss them briefly in § III*b*(ii). We point out some possible tests of these models.

ii) *Emission Processes*

If the approximate continuity of slope and normalization of the infrared and X-ray power laws is not coincidence but has physical significance, what emission mechanisms could explain it? Several possibilities have been discussed in the literature.

1. Direct synchrotron radiation.—Direct synchrotron emission of X-rays is the simplest mechanism, since no reprocessing is needed to make the X-rays. The power-law slope we find for the PG quasars is the same as that of the Crab Nebula, an undoubted synchrotron source, in the X-ray band (1.1 ± 0.03; Toor and Seward 1974). This model leads us to expect strong polarization in both the infrared and the X-ray continua. For radio-quiet PG quasars, it is possible to object to direct X-ray synchrotron emission on the grounds that the radio flux is so low that the synchrotron spectrum must be self-absorbed at high frequencies. This then would lead to a large inverse Compton X-ray flux and so contradict the initial assumption, if their magnetic fields are similar to those in radio-loud quasars. Band and Grindlay (1986) show that this is not necessarily true. They construct a synchrotron self-Compton model for PG 0906+484 which is both consistent with tight millimeter flux limits and still dominated by synchrotron X-rays in the IPC band. Inverse Compton X-rays do not dominate in this model until ~ 20 keV.

It is easy to imagine that the high-energy X-ray surveys pick out the sources where the Compton component dominates and the IPC picks out the sources where synchrotron dominates. Since the importance of the Comptonized component in synchrotron self-Compton models changes rapidly as the parameters of the model (magnetic field, radius) are changed, there may be few intermediate cases. This explanation is independent of the big bump component, so that α_{ox} could be very similar in the two samples.

2. "Unsaturated Comptonization."—In unsaturated Comptonization models (e.g., Maraschi, Roasio, and Treves 1982; Ipser and Price 1983) a seed spectrum is Comptonized into a power law. The power laws produced by this means can easily extend over six decades of frequency. They have indices ranging from ~ 0.5 to ~ 1.0, which is just the range seen in X-rays (excepting PG 1211+143, see Paper II). Steeper slopes can be produced at very small Comptonization parameters, but at these values the spectrum no longer follows a smooth power law but instead reproduces the seed spectrum shifted by successive values of the amplification factor. A power-law slope of ~ 1.0 from infrared to X-ray is in this sense a limiting case for unsaturated Comptonization models.

3. Synchrotron self-Compton.—This has been the most widely discussed mechanism for AGN X-ray emission because the widely seen X-ray slope of 0.7 matches that of the typical high-frequency radio slope of radio-loud AGNs. For an X-ray slope of ~ 1 a different region must provide the photons for upscattering. The only available region is the mid-infrared (2–20 μm). In order to make the apparently continuous IR–X-ray continuum, the primary infrared synchrotron spectrum must fall off in the narrow optical/UV range where it is unobservable because of the big bump thermal emission which dominates there. The resulting scattered X-ray spectrum will then also roll over at high energies (~ 100 keV). A slope of 1.0 from infrared to X-rays implies equal luminosities per decade in the (infrared) synchrotron and (X-ray) inverse Compton components. This is an upper limit to the first-order Compton component (Jones, O'Dell, and Stein 1974*a*, *b*), since any attempt to increase it will instead increase the second-order Compton scattering. In this limiting case the second-order scattering will have the same luminosity as the first-order. This self-limiting process would naturally explain the $\nu f_\nu \approx$ constant nature of the infrared and X-ray flux distributions and the absence of quasars with smaller α_{ox}.

None of these classes of models can be ruled out as yet.

iii) *Optical and X-Ray Obscuration*

For some years argument has raged over the reddening in quasars. The degree of extinction in contention is $A_v \approx 0.1$ and corresponds to small gas columns $\sim 3 \times 10^{20}$ atoms cm^{-2} (see the review by MacAlpine 1985). Previous limits on X-ray column densities were $\sim 3 \times 10^{21}$ atoms cm^{-2} (Reichert *et al.* 1985). No absorption above the Galactic value is seen in our quasar X-ray spectra down to similar values. The maximum allowed intrinsic column density for each quasar is given in Table 4 and has typical values of 4×10^{20} atoms cm^{-2} or less whenever it is usefully constrained. IPC column density measurements are now in the range where they are relevant to the optical reddening debate.

Figure 10 shows the Stark *et al.* (1985) 21 cm Galactic H I column density plotted against the fitted IPC column density. As noted in Appendix B, the comparison of 21 cm $N_{\rm H}$ with that of the IPC is particularly clean, since the IPC is sensitive only to the hydrogen and helium opacities for small column densities. Lines showing additional intrinsic $E(B-V)$ reddening values of 0.05 and 0.10 are shown. This comparison forces assumptions of metallicity and dust-to-gas ratios to be made. The conversion factor used was that of Jenkins and Savage (1974). Five of the eight quasars have intrinsic reddenings less than $E(B-V) = 0.05$ or $\sim 4 \times 10^{20}$ atoms cm^{-2} (Table 4).

It is not clear that these limits imply abnormally low absorption in the host galaxy that we presume to exist for each quasar. The central kiloparsec of even normal face-on galaxies shows a decline in integrated H I column density to levels of only 2–3 $\times 10^{20}$ atoms cm^{-2}. This is illustrated clearly in the series of papers by van der Kruit and Shostak (1984, and references therein). On average, though, galaxies are viewed at 30° inclination, so that the column we would measure would be twice that for face-on galaxies. The intrinsic $N_{\rm H}$ limits that we measure for PG 1501+106 and PG 1307+085 lie below such expected values, but a larger sample is needed to come to more definite conclusions. Our limits do show that we are not viewing these quasars through the disk of an *intervening* normal spiral galaxy.

If we are seeing a deficiency in the X-ray absorbing column, this may be due to the effects of X-rays from a quasar nucleus on the interstellar medium (ISM) of a host galaxy. For luminosities of a few times 10^{44} ergs s^{-1}, similar to those of the quasars considered here, Begelman (1985) finds that the X-rays blow a hole of radius of ~ 1 kpc in the ISM due to radiation

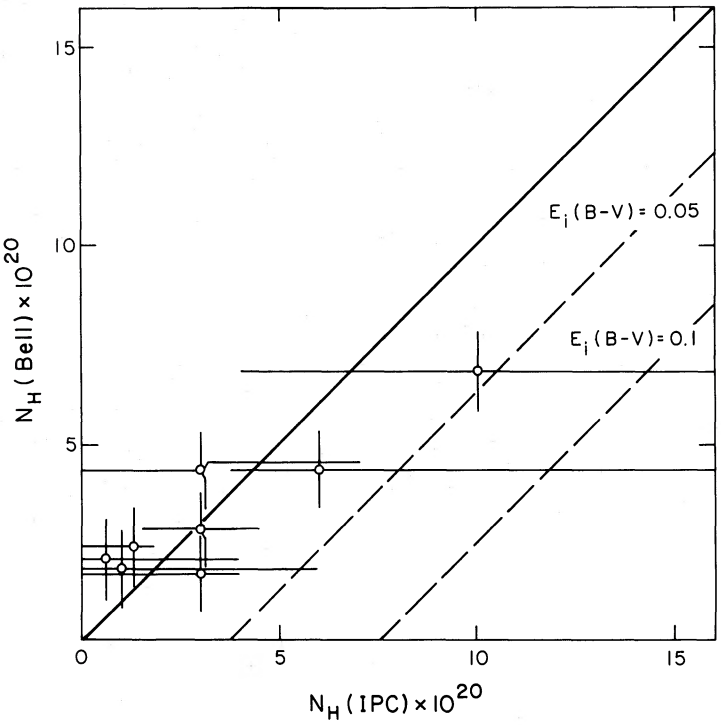

FIG. 10.—Comparison of N_H values measured with the IPC with those derived from the Bell Labs Galactic H I survey (Stark *et al.* 1985). 90% error bars are shown. The solid line is for N_H (IPC) = N_H (Bell). The two dashed lines show lines for *additional* X-ray column density above the Galactic value corresponding to $E(B-V) = 0.05$ and 0.1 (using the conversion of Jenkins and Savage 1974).

pressure. The X-rays also remove the instability that allows cold ($\sim$100 K) clouds in the ISM out to $\sim$10 kpc in this model.

Naively we can also claim from the lack of absorption in any of these eight quasars that the covering factor of both broad and narrow line emitting clouds is less than $\frac{1}{8}$. This is consistent with arguments based on photoionization modeling and on the statistics of optically thick Lyman absorbers (e.g., Kinney *et al.* 1985) but may also be misleading. A column density of 10^{21} atoms cm^{-2} will remove the $\frac{1}{4}$ keV photons and so deprive the IPC of a sufficiently long lever arm to determine a spectrum accurately. A column of $\sim 10^{22}$ atoms cm^{-2}, similar to that of a broad-line region cloud (Kwan and Krolik 1981), will reduce the count rate of an $\alpha = 1.0$ quasar by a factor of $\sim$5–10 and leave only a handful of IPC counts in a typical exposure. We are thus biased against quasars with large intrinsic column densities by our inability to measure their spectra. An unbiased X-ray sample is needed to set a meaningful limit from X-ray measurements on emission-line cloud covering fraction. It would be interesting therefore to apply the battery of proposed emission-line ratio reddening indicators (reviewed by MacAlpine 1985) to this particular set of eight quasars to look for reddening values of a few tenths of $E(B-V)$ suggested for other quasars. This comparison will be begun in Paper III.

We caution that small soft X-ray excesses at $\frac{1}{4}$ keV might mimic low N_H values if the spectra are more complex than a single power-law form. More accurate N_H measurements for our Galaxy, e.g., direct measurement of Lyα absorption for these objects with Space Telescope, would remove some of the uncertainty. Higher quality X-ray spectra will be needed to make definitive statements about the true X-ray column.

IV. CONCLUSIONS

For a sample of eight optically selected (PG) quasars, we find soft X-ray energy spectral indices with a mean value of 1.05 with an observed dispersion of 0.25. In three of the four cases in which we have higher energy data, these steep slopes probably continue to $\sim$6 keV. Five of the eight quasars have X-ray slopes steeper than the canonical 0.7 at 90% confidence. No absorbing column density is seen in excess of the Galactic value with limits of a few times 10^{20}.

These results are at odds both with the "canonical slope" previously seen in AGN X-ray spectra and with the slope of the X-ray background. We conclude that disagreement with previous X-ray slopes is probably due to biases in the selection of the flatter slopes by earlier instruments sensitive to hard X-rays and steeper slopes by the IPC. Soft excesses over a canonical power law may be more common in PG quasars than in hard X-ray selected AGNs. Alternatively, PG quasars may have intrinsically steeper, one-component spectra. The MPC data and the agreement of 21 cm and X-ray column densities favor the latter explanation.

Consideration of the broad-band infrared to X-ray energy distributions of these eight quasars supports the decomposition of these spectra into a "big bump" (accretion disk?) component and a power-law infrared to X-ray continuum. The "big bump" and power-law components always cross over in νf_ν at ~ 1 μm in these quasars. This seems to imply a luminosity balance between the two components.

A continuity of the infrared and X-ray power laws in slope and normalization is consistent with the data. This suggests that a single power law covers five decades of frequency. This

continuity is further, limited evidence for intrinsically steep X-ray spectra in PG quasars. This broad-band continuum can be modeled with any of direct synchrotron, unsaturated Comptonization, or synchrotron self-Compton processes as candidate emission mechanisms.

The lack of absorption in these quasars suggests that their host galaxies are not normal spirals. Quite plausibly, the X-ray radiation of the quasar has altered or removed the ISM in the central regions of these objects. We do not know whether lack of absorption is a general property of quasar X-ray spectra, because the IPC is biased against heavily absorbed sources. Better X-ray spectra are essential to rule out weak soft excesses that would mimic low N_H.

Larger samples of broad-band energy distributions of quasars are needed. The IPC will provide a good starting point for this by providing ~ 50 quasar spectra in all. Complete well-defined samples of optically selected quasars are needed to provide unbiased answers to the questions raised in this paper. ROSAT will be able to provide such samples at low energies in spite of its lack of response above 2 keV, thanks to the extreme lack of low-energy absorption in quasars. Higher energy spectra are important for the question of the contribution of quasars to the X-ray background. EXOSAT will begin to provide these. Only when the large area and bandwidth of AXAF become available will high-resolution X-ray spectra become available. At that point we will be able to go beyond simple power-law models and investigate the full complexity of the quasar X-ray spectra.

We thank David Band, Leo Blitz, Bożena Czerny, John Dickey, Tom Jones, Julian Krolik, Richard Mushotzky, Mike Watson, and Belinda Wilkes for useful discussions and Bill Keel, Mike Sitko, and Harvey Tananbaum for use of their data in advance of publication. We thank the referee for helpful criticism. We also thank R. Kondo and C. Poux for assistance in the *Einstein* data analysis.

This work was supported in part by NASA contract NAS8-30751 and by the National Science Foundation under grant AST-8314143. Infrared astrophysics at Caltech is supported by NSF grant A3-12699.

APPENDIX A

RELATIVE CALIBRATION OF THE IPC AND MPC

The natural method of cross-calibrating these two instruments is to take bright sources (to avoid the systematic background uncertainties in the MPC) and fit the same spectrum to each instrument separately. For the same spectral form (e.g., $[\alpha_E, N_H]$ values), the normalizations derived for the two instruments should agree if a simple spectrum provides a good fit over the 0.1–10 keV band.

It is surprisingly hard to find suitable sources. The bright galactic sources mostly have large ($>10^{21}$ atoms cm^{-2}) column densities, which makes the temperature or slope indeterminate in the IPC. Also, the IPC was made to avoid such sources because of the danger of producing a breakdown in the counter. The Crab Nebula, and other supernova remnants, are extended sources and we are interested in the IPC calibration for point sources, which is differently derived (Harnden and Fabricant 1985). Clusters of galaxies must be excluded, since they too are extended.

We concentrated on BL Lac objects and Seyfert galaxies, of which several have MPC count rates above 2 counts s^{-1}. The MPC background uncertainty of ~ 0.07 counts s^{-1} is thus $\sim 5\%$ for these sources. Not all these sources could be well fitted by a single power law. We are eventually left with eight observations satisfying these constraints. Table 9 shows the results. The observation sequence number, source name, and MPC exposure time (ksec) and count rate are given for reference. The important quantity is I/M. This is the ratio of the normalization given by the IPC to that in the MPC for the same (α_E, N_H) values. This is the same as the ratio of the fluxes predicted at 1 keV in each instrument. These I/M values have a mean of 1.01 and a standard deviation of 0.13. The most deviant point is that for NGC 7469, for which there is evidence (see § III*a* and Fig. 3) for a steepening in slope from the hard to the soft X-ray bands. At 1 keV this would depress the MPC normalization with respect to the IPC. In Table 9 the opposite effect is observed. If NGC 7469 is eliminated, the remaining points have a mean of 1.04 and a standard deviation of 0.10. Although there are fewer points than we would like, it is clear that the deviation in the normalization ratios is similar to the uncertainty introduced by the MPC background error in these sources. The cross-calibration of the IPC and MPC is thus good to better than around 10%.

For sources at ~ 0.5 MPC counts s^{-1}, such as our quasars, it is the MPC background uncertainty which dominates. We have included an extra 10% error, added in quadrature, to allow for residual IPC/MPC cross-calibration errors.

TABLE 9

IPC/MPC CROSS-CALIBRATION

Observation Sequence No.	Source Name	MPC Exposure (ks)	MPC Counts s^{-1}	I/M
2074.....	MR 2251−179	1.23	2.18	1.04
1978.....	NGC 7469	2.04	2.10	0.77
356.....	NGC 5548	18.56	2.18	0.94
5208.....	Mrk 421	3.66	2.52	1.01
5211.....	Mrk 501	1.44	3.60	1.03
7726.....	PKS 0548−322	2.18	2.44	1.08
2037.....	3C 273	1.25	5.57	1.25
9310.....	3C 273	2.66	10.54	0.95

APPENDIX B

THE UNCERTAINTY IN THE BELL LABS GALACTIC N_H FOR COMPARISON WITH X-RAY COLUMN DENSITY MEASUREMENTS

The great sensitivity of the IPC in the $\frac{1}{4}$ keV band makes the exact value of the column density through our own Galaxy highly significant for X-ray spectral fitting. In particular, we need to determine the error associated with the Bell Labs 21 cm H I survey of Stark *et al.* (1985), since this survey provides the best all-sky data on the Galactic column density.

For the small column densities of a few times 10^{20} atoms cm^{-1} to which we are sensitive with the IPC, it is the transmission below the 0.3 keV (42 Å) carbon edge (see Harnden and Fabricant 1985) which determines the X-ray column density. (This is shown clearly in Figs. 8.2 and 8.3 in Gorenstein 1974.) Below this edge the only significant opacity is due to hydrogen and helium (see, e.g., Fig. 1 in Morrison and McCammon 1983). This makes the line-of-sight H I column an unusually direct estimate of the Galactic X-ray opacity for the IPC, since the normally necessary assumptions concerning abundances and dust-to-gas ratios (summarized in Maccacaro, Perola, and Elvis 1982) are not relevant.

Two potential problems remain:

i) The existence of high-latitude H_2 in a nearby molecular cloud along the line of sight.

ii) Small-scale structure in the integrated H I column.

An unbiased survey of high-latitude CO emission (Magnani, Blitz, and Lada 1985) gives a chance of 1 in 220 of intercepting one of

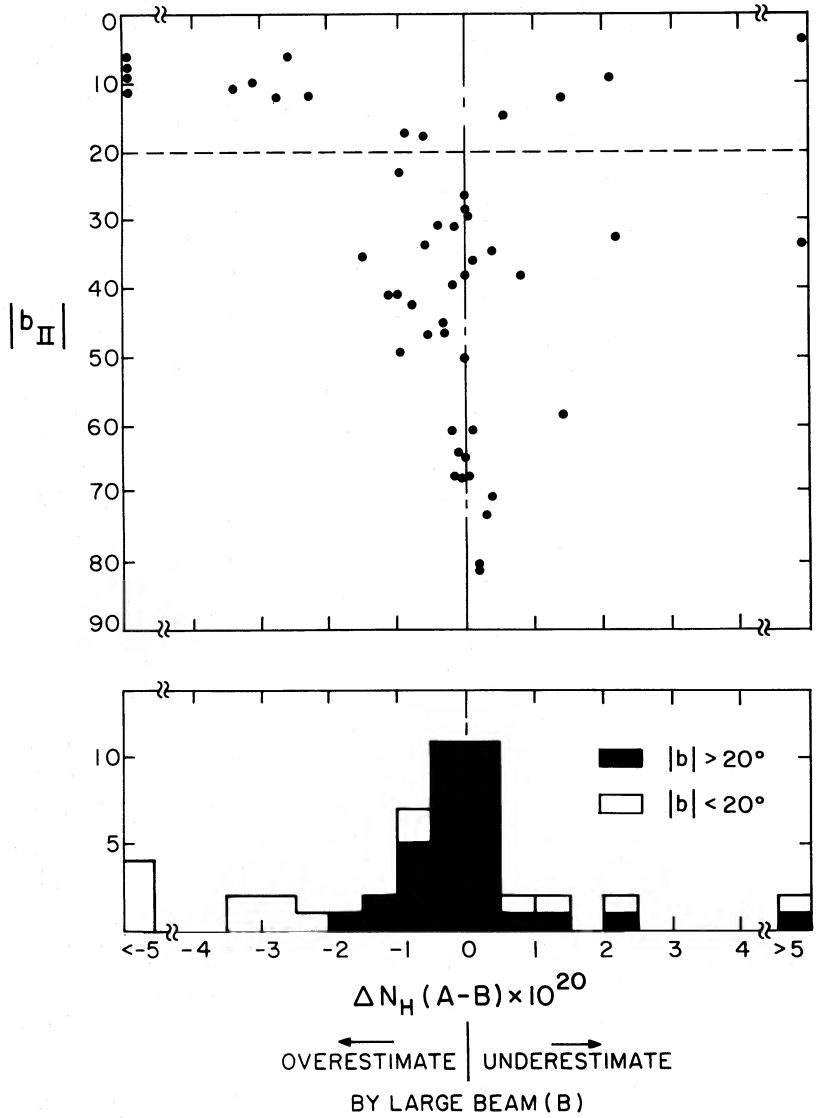

FIG. 11.—Difference between Arecibo ("A," 3′ FWHM) and Bell labs ("B," 2° FWHM) measurements of column density. *Top*, differences vs. Galactic latitude. *Bottom*, data compressed into a histogram, with the solid area for points at $|b| > 20°$.

the high-latitude CO clouds discussed by Blitz, Magnani, and Mundy (1984). This suggests that the chance of intercepting a large column of H_2 is small. (Note, however, that because the detected clouds are large, one does expect to detect them in an all-sky survey of soft X-ray absorption.) *Copernicus* H_2 absorption line measurements (Savage *et al.* 1977, Table 3) show that outside the high-latitude CO clouds, it is unlikely that the column of H_2 exceeds 5% of the H I column and may be much less ($\sim 10^{-5}$).

We have considered the problem of small-scale structure more carefully with respect to the Stark *et al.* 21 cm survey. The Bell Labs H I antenna has very low sidelobes so that the problem of stray radiation is negligible. However, it has a large primary beam (HPBW $\approx 2°$). Any spatial structure in the H I column on smaller scales will lead to random errors between the Bell Labs value of N_H for a given point in the sky and the actual value. We have compared the large-beam Stark *et al.* values with small-beam (HPBW = 3′) Arecibo measurements (Dickey, Salpeter, and Terzian 1978; Payne, Salpeter, and Terzian 1982; Table 10). Figure 11 illustrates this comparison. For $|b| > 20°$ the distribution of differences is symmetrical about 0.0, implying that the two surveys are well calibrated, at least with respect to one another. The distribution has a standard deviation of 0.7×10^{20} atoms cm^{-2}.

TABLE 10

COMPARISON OF LARGE-BEAM AND SMALL-BEAM N_H VALUES

Name	R.A. (1950)	Decl. (1950)	b	*A* N_H (Arecibo) ($\times 10^{20}$)	*B* N_H (Bell) ($\times 10^{20}$)	$A-B$ ($\times 10^{20}$)
3C 48	01^{h}34^{m}49^s.8	32°54′21″	−28.7	4.4	4.4	0.0
CTA 21	03 16 09.1	16 17 41	−33.6	9.9	10.5	−0.6
3C 111	4 15 01.1	37 54 37	−8.8	30.8	28.7	+2.1
3C 123	4 33 55.2	29 34 14	−11.7	16.4	18.7	−2.3
3C 133	4 59 54.2	25 12 12	−9.9	25.3	28.4	−3.1
3C 138	5 18 16.5	16 35 26	−11.3	14.2	23.9	−9.7
PKS 0531+19	5 31 47.4	19 25 18	−7.1	18.4	31.5	−13.1
3C 237	10 05 22.1	7 44 58	+46.6	2.3	2.6	−0.3
3C 264	11 42 32.1	19 53 56	+73.1	2.5	2.2	+0.3
3C 270	12 16 51.2	6 06 13	+67.4	1.4	1.6	−0.2
3C 273	12 26 32.9	2 19 39	+64.4	1.8	1.8	0.0
3C 287	13 28 16.0	25 24 37	+81.0	1.3	1.1	+0.2
3C 286	13 28 49.7	30 46 02	+80.7	1.4	1.2	+0.2
PKS 1345+12	13 45 06.3	12 32 23	+70.2	2.3	1.9	+0.4
3C 298	14 16 38.8	6 42 23	+60.7	2.0	2.2	−0.2
3C 310	15 02 48.0	26 12 36	+60.2	3.6	3.5	+0.1
3C 317	15 14 17.0	7 12 17	+50.1	2.9	2.9	0.0
3C 327	15 59 56.0	2 06 16	+37.9	6.3	6.3	0.0
3C 348	16 48 40.1	5 04 28	+28.9	5.4	6.3	−0.9
3C 382	18 33 12.5	32 39 11	+17.4	6.5	7.4	−0.9
3C 386	18 36 12.4	17 09 10	+10.5	15.1	18.5	−3.4
3C 409	20 12 18.2	23 25 42	−6.1	22.0	29.6	−7.6
3C 433	21 21 30.6	24 51 18	−17.7	7.9	8.5	−0.6
PKS 2247+14	22 47 56.8	14 03 56	−39.2	4.6	4.8[a]	−0.2[a]
3C 454.0	22 49 07.8	18 32 44	−35.6	4.3	5.8	−1.5
3C 454.3	22 51 29.4	15 52 56	−38.2	7.2	6.4	+0.8
3C 455	22 52 34.6	12 57 36	−40.7	4.1	5.1	−1.0
3C 33	01 06 14.2	13 03 37	−49.3	2.95	3.9	−0.95
3C 47	01 33 40.0	20 41 55	−40.7	4.67	5.8	−1.13
3C 75	02 55 05.1	05 50 44	−44.9	8.48	8.8	−0.32
3C 76.1	03 00 27.1	16 14 31	−36.0	10.21	10.1	+0.11
3C 79	03 07 11.4	16 54 34	−34.5	10.41	10.0	+0.41
3C 98	03 56 11.0	10 17 41	−31.1	11.43	11.6	−0.17
3C 105	04 04 44.8	03 33 26	−33.6	20.65	11.7	+8.95
3C 123	04 33 55.2	29 34 14	−11.7	20.12	18.7	+1.42
3C 192	08 02 35.1	24 18 34	+26.4	4.29	4.3	−0.01
3C 200	08 24 21.6	29 28 36	+32.6	6.02	3.8	+2.22
3C 227	09 45 07.8	07 39 09	+42.3	2.12	2.9	−0.78
3C 237	10 05 22.1	07 44 58	+46.6	2.05	2.6	−0.55
3C 270W	12 16 41.0	06 06 14	+67.4	1.60	1.6	0.0
3C 270E	12 17 01.2	06 06 14	+67.4	1.62	1.6	+0.02
PKS 1414+11	14 14 27.3	11 02 16	+64.1	1.80	1.9	−0.10
3C 315	15 11 31.0	26 18 37	+58.3	5.22	3.8	+1.44
3C 357	17 26 27.0	31 48 25	+30.6	3.03	3.4	−0.37
PKS 1739+17	17 39 26.9	17 21 58	+23.0	5.14	6.1	−0.96
PKS 1820+17	18 20 09.0	17 58 34	+14.4	16.26	15.7[a]	+0.56[a]
3C 390	18 43 15.4	09 50 29	+5.8	26.92	29.5	−2.58
3C 395	19 01 02.2	31 55 13	+11.8	8.35	11.1[a]	−2.75[a]
4C 33.48	19 22 25.1	33 23 35	+8.4	12.25	17.2	−4.95
3C 410	20 18 03.9	29 32 49	−3.8	53.20	43.5	+9.70

[a] Not enough N_H grid points for interpolation to the source position. The nearest grid point to the source was used.

Between a scale of 2° and 3′ there is thus a typical 90% (1.65 σ) error of $\pm 1 \times 10^{20}$ atoms cm^{-2}. This small value agrees with the observation of Kalberla, Schwarz, and Goss (1985), who find that "most of the observed H I gas [toward 3C 147] is extended on scales >10 arc min." Kalberla *et al.* do find weaker structure down to the 3′ scale of the Arecibo beam. Between 3′ and the approximately nanoarcsecond size of the quasar continuum source, there is, in principle, scope for further uncertainties. This possibility was investigated by Payne, Salpeter, and Terzian (1982). They compared H I absorption and emission ratios toward radio galaxies extended by arcminutes with those toward compact (<arcseconds) radio galaxies (Dickey, Salpeter, and Terzian 1978) and concluded that there was no difference in the ratios, implying little small-scale structure. The same conclusion was reached by Dickey (1981), who used pulsars as his "point" sources. It seems that most of the ISM structure has been resolved out with the 3′ Arecibo beam.

Physically, 3′ corresponds to a typical ISM scale of 0.3 pc (assuming a Galactic H I scale height of 250 pc and looking at $|b| \geq 20°$). The ISM does seem to be rather smooth on scales smaller than this. Crovisier, Dickey, and Kazes (1985) have shown that large deviations of N_H on scales less than ~ 1 pc are rare. Another way of expressing this is to say that the power spectrum of H I spatial structure declines steeply to high frequencies. Crovisier and Dickey (1983) find a slope of -2.5 for this power spectrum.

There are known to be filamentary structures below the 3′ scale that may still produce some low-level uncertainty in the absorbing column. In emission, examples are the faint reflection nebulae described by Sandage (1976) and the *IRAS* cirrus (Low *et al.* 1984). It is not clear yet how thick these filaments are in N_H. Our results suggest that they should have $N_H \lesssim 10^{20}$ atoms cm^{-2}. Shull and Van Steenberg (1985) note that none of the 17 stars that lie more than 1 kpc out of the disk have $N_H < 10^{20}$ atoms cm^{-2}, which suggests that small-scale holes in the ISM are rare.

Overall we conclude that our error estimate of $\pm 1 \times 10^{20}$ atoms cm^{-2} (90% confidence) is likely to be a good estimate of the Galactic column uncertainty associated with the Bell Labs' survey.

REFERENCES

Arnaud, K. A., *et al.* 1985, *M.N.R.A.S.*, **217**, 105.
Avni, Y. 1976, *Ap. J.*, **210**, 642.
Avni, Y., and Tananbaum, H. 1986, *Ap. J.*, **305**, 83.
Band, D., and Grindlay, J. E. 1986, *Ap. J.*, **308**, 576.
Barbieri, C., Cristiani, S., and Romano, G. 1982, *Ap. J.*, **87**, 616.
Bechtold, J., Czerny, B., Elvis, M., Fabbiano, G., and Green, R. F. 1985, *Ap. J.*, submitted (Paper II).
Begelman, M. 1985, *Ap. J.*, **297**, 492.
Blitz, L. Magnani, L., and Mundy, L. 1984, *Ap. J.* (*Letters*), **282**, L9.
Boggess, A., *et al.* 1978*a*, *Nature*, **275**, 372.
Boggess, A., *et al.* 1978*b*, *Nature*, **275**, 377.
Bohlin, R. C. 1978, *Ap. J.*, **224**, 132.
Bohlin, R. C., *et al.* 1980, *Astr. Ap.*, **85**, 1.
Brown, R. L., and Gould, R. J. 1970, *Phys. Rev.*, **D2**, 2252.
Cheng, F. Z., Danese, L., DeZotti, G., and Lucchin, F. 1984, *M.N.R.A.S.*, **208**, 799.
Crovisier, J., and Dickey, J. M. 1983, *Astr. Ap.*, **122**, 282.
Crovisier, J., Dickey, J. M., and Kazes, I. 1985, *Astr. Ap.*, **146**, 223.
Cutri, R. M., Wisniewski, W. Z., Rieke, G. H., and Lebofsky, M. J. 1985, *Ap. J.*, **296**, 423.
Dickey, J. M. 1981, *Astr. Ap.*, **107**, 332.
Dickey, J. M., Salpeter, E., and Terzian, Y. 1978, *Ap. J. Suppl.*, **36**, 77.
Elias, J. H., Frogel, J. A., Matthews, K., and Neugebauer, G. 1982, *A.J.*, **87**, 1029.
Elvis, M. 1985, in *Compact Galactic and Extragalactic X-ray Sources, Japan–U.S. Seminar*, ed. Y. Tanaka and W. H. G. Lewin (Tokyo: ISAS), p. 291.
Elvis, M., and Lawrence, A. 1985, in *Astrophysics of Active Galaxies and Quasi-Stellar Objects*, ed. J. S. Miller (Mill Valley, CA: University Science Books), p. 289.
Elvis, M., Wilkes, B. W., and Tananbaum, H. 1985, *Ap. J.*, **292**, 357.
Forman, W., *et al.* 1978, *Ap. J. Suppl.*, **38**, 357.
Giacconi, R., *et al.* 1979, *Ap. J.*, **230**, 540.
Gioia, I. M., *et al.* 1984, *Ap. J.*, **283**, 495.
Gorenstein, P. 1974, in *X-Ray Astronomy*, ed. R. Giacconi and H. Gursky (Dordrecht: Reidel), p. 299.
Gorenstein, P., Harnden, R. F., Jr., and Fabricant, D. 1981, *IEEE Trans.*, **NS-28**, 869.
Grandi, S. 1982, *Ap. J.*, **255**, 25.
Green, R. F., *et al.* 1985, in preparation (Paper III).
Green, R. F., Schmidt, M., and Liebert, J., 1986, *Ap. J. Suppl.*, **61**, 305 (PG).
Halpern, J. P. 1982, Ph.D. thesis, Harvard University.
Halpern, J. P., and Filippenko, A. V. 1984, *Ap. J.*, **285**, 485.
Harnden, F. R., Jr., and Fabricant, D. 1986, in preparation.
Ipser, J. R., and Price, R. H. 1983, *Ap. J.*, **267**, 371.
Jenkins, E. B., and Savage, B. D. 1974, *Ap. J.*, **187**, 243.
Jones, T. W., O'Dell, S. L., and Stein, W. A., 1974*a*, *Ap. J.*, **188**, 353.
———. 1974*b*, *Ap. J.*, **192**, 261.
Kalberla, P. M. W., Schwarz, U. J., and Goss, W. M. 1985, *Astr. Ap.*, **144**, 27.
Kazanas, D. 1984, *Ap. J.*, **287**, 112.
Kinney, A. L., Huggins, P. J., Bregman, J. N., and Glassgold, A. E. 1985, *Ap. J.*, **291**, 128.
Kriss, G. A., Cioffi, D. F., and Canizares, C. R. 1983, *Ap. J.*, **272**, 439.
Krolik, J. H., McKee, C. F., and Tarter, C. B. 1981, *Ap. J.*, **249**, 422.
Kwan, J. Y., and Krolik, J. H. 1981, *Ap. J.*, **250**, 478.
Lawrence, A., and Elvis, M. 1982, *Ap. J.*, **253**, 410.
Low, F. J., *et al.* 1984, *Ap. J.* (*Letters*), **278**, L19.
MacAlpine, G. M. 1985, in *Astrophysics of Active Galaxies and Quasi-Stellar Objects*, ed. J. S. Miller (Mill Valley, CA: University Science Books), p. 259.
Maccacaro, T., Perola, G. C., and Elvis, M. 1982, *Ap. J.*, **257**, 47.
Magnani, L., Lada, E., and Blitz, L. 1985, *Ap. J.*, **301**, 395.
Malkan, M. A., and Sargent, W. L. W. 1982, *Ap. J.*, **254**, 22.
Maraschi, L., Roasio, R., and Treves, A. 1982, *Ap. J.*, **253**, 312.
Marshall, H., Avni, Y., Braccesi, A., Huchra, J. P., Tananbaum, H., Zamorani, G., and Zitelli, V. 1984, *Ap. J.*, **283**, 50.
Marshall, F. E., Boldt, E. A., Holt, S. S., Miller, R. B., Mushotzky, R. F., Rose, L. A., Rothschild, R. E., and Serlemitsos, P. J. 1980, *Ap. J.*, **235**, 4.
Mészáros, P. 1983, *Ap. J.* (*Letters*), **274**, L13.
Morrison, R., and McCammon, D. 1983, *Ap. J.*, **270**, 119.
Mushotzky, R. F. 1982, *Ap. J.*, **256**, 92.
———. 1984, *Adv. Space Res.*, Vol. **3** No. 10–13, p. 157.
Mushotzky, R. F., and Marshall, F. E. 1980, *Ap. J.* (*Letters*), **239**, L5.
Mushotzky, R. F., Marshall, F. E., Boldt, E. A., Holt, S. S., and Serlemitsos, P. J. 1980, *Ap. J.*, **235**, 377.
Nousek, J. A., Fried, P. M., Sanders, W. T., and Kraushaar, W. L. 1982, *Ap. J.*, **258**, 83.
Oke, J. B. 1969, *Pub. A.S.P.*, **81**, 11.
Oke, J. B., and Gunn, J. 1983, *Ap. J.*, **266**, 713.
Payne, H. E., Salpeter, E. E., and Terzian, Y., 1982, *Ap. J.*, Suppl., **48**, 199.
Petre, R., Mushotzky, R. F., Krolik, J. H., and Holt, S. S. 1984, *Ap. J.*, **280**, 499.
Piccinotti, G., Mushotzky, R. F., Boldt, E. A., Holt, S. S., Marshall, F. E., Serlemitsos, P. J., and Shafer, R. A. 1982, *Ap. J.*, **253**, 485.
Pounds, K. A. 1985, in *Galactic and Extragalactic Compact X-Ray Sources*, ed. Y. Tanaka and W. H. G. Lewin (Tokyo: ISAS), p. 261.
Puetter, R. C., Burbidge, E. M., Smith, H. E., and Stein, W. A. 1982, *Ap. J.*, **257**, 487.
Raymond, J. 1980, private communication.
Raymond, J., and Smith, B. W. 1977, *Ap. J. Suppl.*, **35**, 419.
Reichert, G. A., Mushotzky, R. F., Petre, R., and Holt, S. S. 1985, *Ap. J.*, **296**, 69.
Richstone, D. O., and Schmidt, M., 1980, *Ap. J.*, **235**, 361.
Rothschild, R. E., Mushotzky, R. F., Baity, W. A., Gruber, D. E., Matteson, J. L., and Primini, F. A. 1983, *Ap. J.*, **269**, 423.
Sandage, A. 1976, *A.J.*, **81**, 954.
Savage, B., *et al.* 1977, *Ap. J.*, **216**, 291.
Schlosman, I., Shaham, J., and Shaviv, G. 1984, *Ap. J.*, **287**, 534.
Schmidt, M. 1968, *Ap. J.*, **151**, 393.
Schmidt, M., and Green, R. F. 1983, *Ap. J.*, **269**, 352.
———. 1986, *Ap. J.*, **305**, 68.
Seaton, M., 1979, *M.N.R.A.S.*, **187**, 73P.
Shields, G. A. 1978, *Nature*, **272**, 706.
Shull, J. M., and VanSteenberg, M. E. 1985, *Ap. J.*, **294**, 599.
Stark, A. A., Heiles, C., Bally, J., and Linke, R., 1986, in preparation.
Tananbaum, H., Avni, Y., Green, R. F., Schmidt, M., and Zamorani, G. 1986, *Ap. J.*, **305**, 59.
Toor, A., and Seward, F. D. 1974, *A.J.*, **79**, 995.
Turnrose, B. E., and Perry, P. M. 1977, *IUE Image Processing Overview* (Silver Springs, MD: Computer Sciences Corporation, NASA/GSFC).
van der Kruit, P. C., and Shostak, G. S. 1984, *Astr. Ap.*, **134**, 258.

Véron-Cetty, M. D., and Véron, P., 1985, ESO Sci. Rept., No. 4.
Ward, M. J., Elvis, M., Fabbiano, G., Carleton, N. P., Willner, S. P., and Lawrence, A., 1986, *Ap. J.*, submitted.
White, N. E., Fabian, A. C., and Mushotzky, R. F. 1984, *Astr. Ap.*, **133**, L9.
Wills, B. J., Netzer, H., and Wills, D. 1985, *Ap. J.*, **288**, 94.
Yee, H. K. C., and Green, R. F. 1984, *Ap. J.*, **280**, 79.
Zamorani, G., *et al.* 1981, *Ap. J.*, **245**, 357.
Zamorani, G., Giommi, P., Maccacaro, T., and Tananbaum, H. 1984, *Ap. J.*, **278**, 28.
Zdziarski, A., and Lightman, A. P. 1985, *Ap. J.* (*Letters*), **294**, L79.

J. BECHTOLD: Mt. Wilson and Las Campanas Observatories, Carnegie Institution of Washington, 813 Santa Barbara Street, Pasadena, CA 91101

M. ELVIS and G. FABBIANO: Harvard-Smithsonian Center for Astrophysics, 60 Garden Street, Cambridge, MA 02138

R. GREEN: NOAO-KPNO, P.O. Box 26732, Tucson, AZ 85726

K. MATHEWS, G. NEUGEBAUER, M. SCHMIDT, and B. T. SOIFER: California Institute of Technology, Pasadena, CA 91125